iScience

CellPress

Article

TRAF6 Plays a Proviral Role in Tick-Borne Flavivirus Infection through Interaction with the NS3 Protease

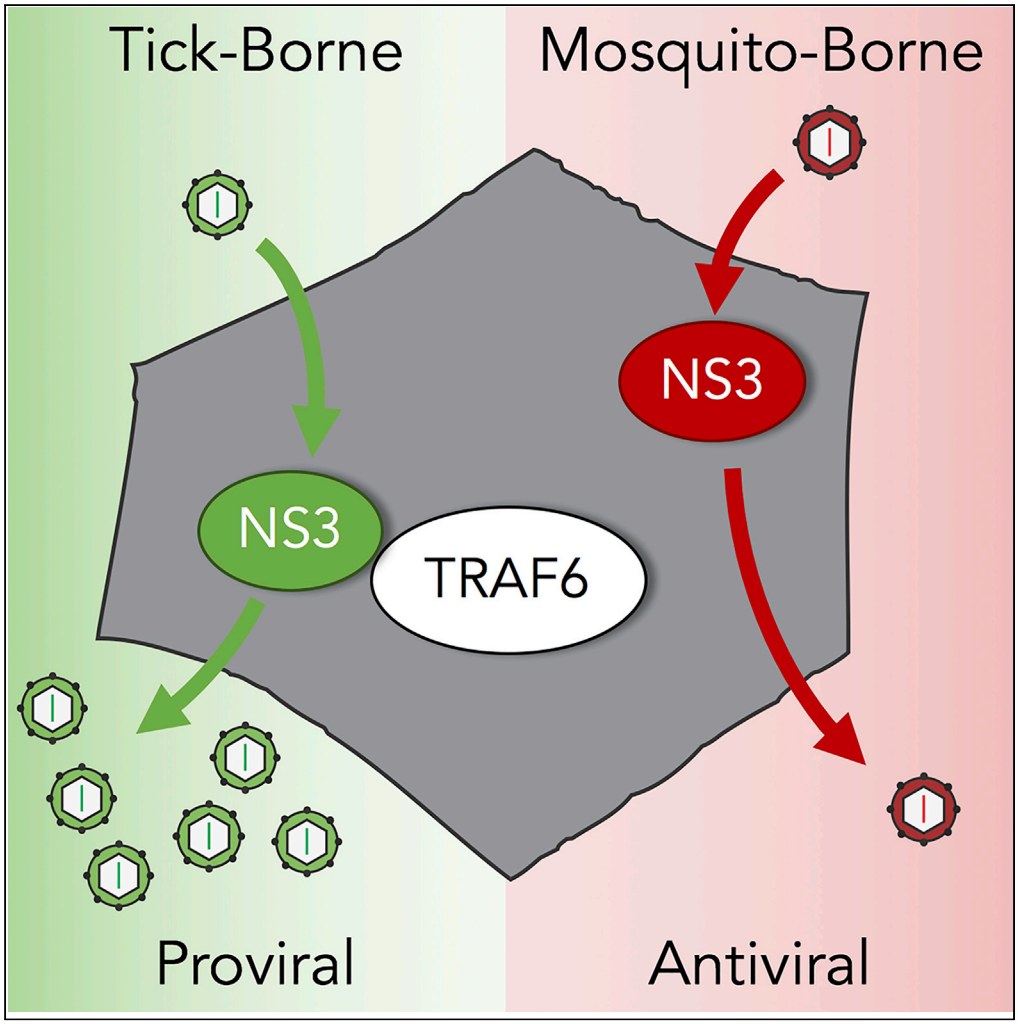

Brian H. Youseff, Thomas G. Brewer, Kristin L. McNally, ..., Sonja M. Best, Xiche Hu, R. Travis Taylor

travis.taylor@utoledo.edu

HIGHLIGHTS

Langat virus (LGTV) NS3 protease interacts with TRAF6 during infection

Tick-borne, unlike mosquito-borne, flaviviruses use TRAF6 for optimal replication

E117A mutation of LGTV NS3 reduces TRAF6 binding and mature protease abundance

LGTV with a mutated TRAF6-binding motif is attenuated *in vitro*

Youseff et al., iScience *15*, 489–501
May 31, 2019
https://doi.org/10.1016/j.isci.2019.05.010

iScience

CellPress

Article

TRAF6 Plays a Proviral Role in Tick-Borne Flavivirus Infection through Interaction with the NS3 Protease

Brian H. Youseff,[1] Thomas G. Brewer,[1] Kristin L. McNally,[3] Adaeze O. Izuogu,[1] Kirk J. Lubick,[3] John B. Presloid,[1] Saad Alqahtani,[2] Saurabh Chattopadhyay,[1] Sonja M. Best,[3] Xiche Hu,[2] and R. Travis Taylor[1,4,*]

SUMMARY

Tick-borne flaviviruses (TBFVs) can cause life-threatening encephalitis and hemorrhagic fever. To identify virus-host interactions that may be exploited as therapeutic targets, we analyzed the TBFV polyprotein *in silico* for antiviral protein-binding motifs. We obtained two putative tumor necrosis factor receptor-associated factor 6 (TRAF6)-binding motifs (TBMs) within the protease domain of the viral nonstructural 3 (NS3) protein. Here, we show that TBFV NS3 interacted with TRAF6 during infection and that TRAF6 supports TBFV replication. The proviral role of TRAF6 was not seen with mosquito-borne flaviviruses, consistent with the lack of conserved TBMs. Mutation of the second TBM within NS3 disrupted TRAF6 binding, coincident with reduced abundance of mature, autocatalytically derived form of the NS3 protease and significant virus attenuation *in vitro*. Our studies reveal insights into how flaviviruses exploit innate immunity for the purpose of viral replication and identify a potential target for therapeutic design.

INTRODUCTION

Viruses within the *Flavivirus* genus represent an overwhelming disease burden to humans, in worst cases causing either encephalitis or hemorrhagic fever with mortality rates up to 50% (Leyssen et al., 2000). The success of flaviviruses is in large part associated with transmission by arthropod vectors, either mosquito borne, represented by dengue virus (DENV), West Nile virus (WNV), and Zika virus, or tick borne, including tick-borne encephalitis virus (TBEV), Omsk hemorrhagic fever virus, Kyasanur Forest disease virus (KFDV), and Powassan virus (POWV). No specific antiviral therapy is available for the millions of individuals infected with flaviviruses each year. We rationalize that to develop desperately needed drugs and vaccines to treat and prevent flavivirus infections, we need to better understand how flaviviruses infect cells and cause disease.

The flavivirus chymotrypsin-like serine protease, nonstructural 3 (NS3), is an ideal target for broad-spectrum antiviral development (Luo et al., 2015). NS3 is relatively conserved between the flaviviruses and is essential for virus replication, functioning to cleave the viral polyprotein into mature individual proteins through a well-characterized enzymatic function (Li et al., 2014; Palanisamy et al., 2018). Mutant flaviviruses with an inactive NS3 protease are unable to generate infectious virions (Chambers et al., 2005). Despite substantial effort and resources directed toward the design of NS3 protease inhibitors, there has only been limited success and no compound has reached the clinical trial stage (Brecher et al., 2017). Innovative discovery approaches seek to expand potential drug targets by identifying protein-protein interactions necessary for viral protein function during infection (Geiss et al., 2009). We reasoned here that the identification of host proteins that interact with NS3 may direct us toward methods to inhibit NS3, either by modeling antiviral drugs from host antiviral interactions with NS3, or by identifying host proteins that NS3 uses during infection.

Bioinformatic analysis of the TBEV polyprotein revealed a potential interaction with the host protein tumor necrosis factor receptor-associated factor 6 (TRAF6). TRAF6 is an important antiviral intracellular molecule for the interleukin-1(IL-1)/Toll-like receptor (TLR) and retinoic acid-inducible gene I (RIG-I) signaling pathways (Inoue et al., 2007; Wu and Arron, 2003; Yoshida et al., 2008). It functions by linking innate immune receptor engagement to activation of protein kinase complexes, culminating in activation of transcription factors including nuclear factor-κB (NF-κB) and activator protein-1 (Walsh et al., 2015). TRAF6 is an E3

[1]Department of Medical Microbiology and Immunology, University of Toledo College of Medicine and Life Sciences, Toledo, OH 43614, USA

[2]Department of Chemistry and Biochemistry, University of Toledo, Toledo, OH 43606, USA

[3]Innate Immunity and Pathogenesis Unit, Laboratory of Virology, Rocky Mountain Laboratories, DIR, NIAID, NIH, Hamilton, MT 59840, USA

[4]Lead Contact

*Correspondence: travis.taylor@utoledo.edu

https://doi.org/10.1016/j.isci.2019.05.010

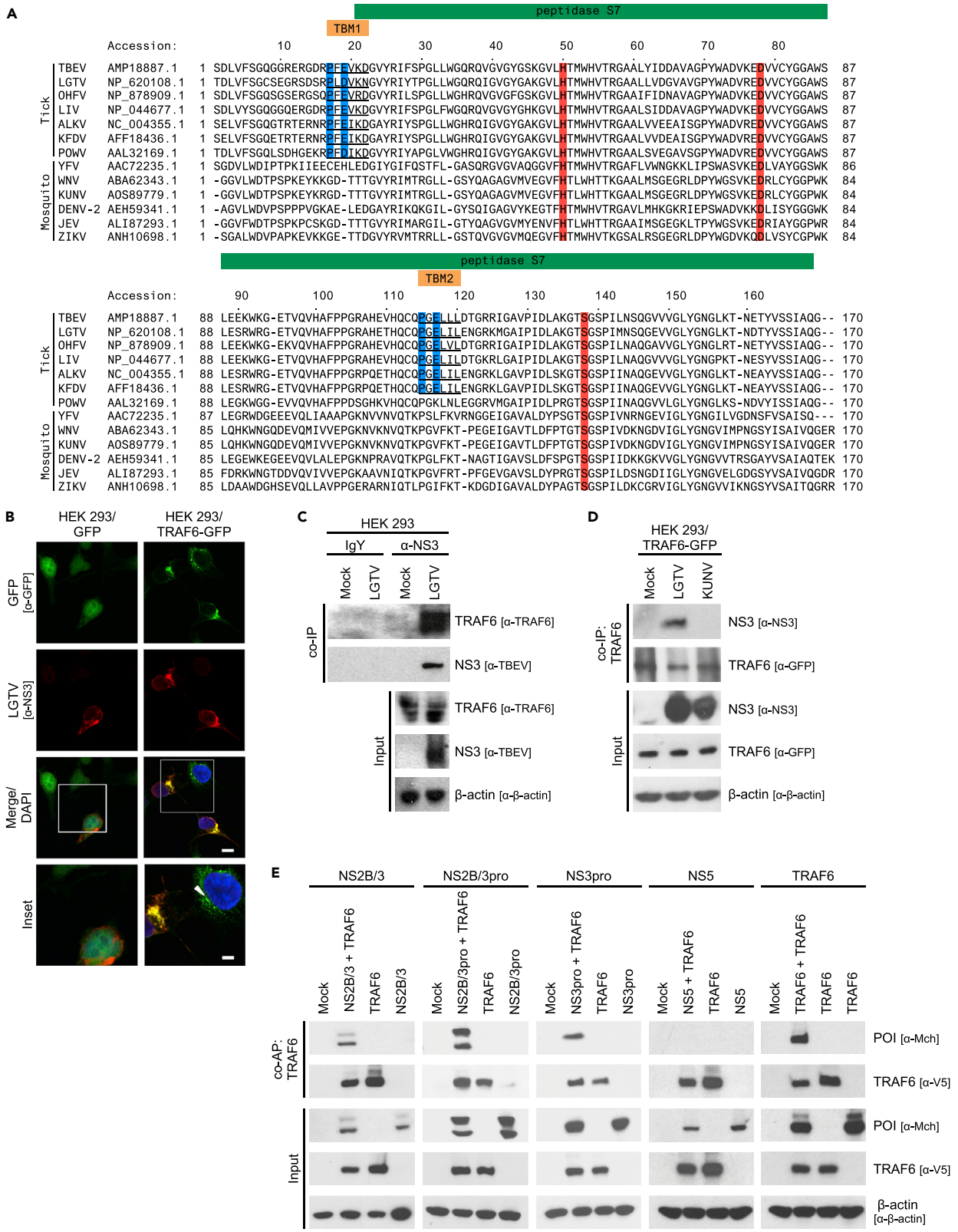
A
peptidase S7
TBM1
Accession:
10 20 30 40 50 60 70 80
Tick
Mosquito
TBEV AMP18887.1 1 SDLVFSGQGGRERGDRPFEVKDGVYRIFSPGLLWGQRQVGVGYGSKGVLHTMWHVTRGAALYIDDAVAGPYWADVKEDVVCYGGAWS 87
LGTV NP_620108.1 1 TDLVFSGCSEGRSDSRPLDVKNGVYRIYTPGLLWGQRQIGVGYGAKGVLHTMWHVTRGAALLVDGVAVGPYWADVREDVVCYGGAWS 87
OHFV NP_878909.1 1 SDLVFSGQSGSERGSQPFEVRDGVYRILSPGLLWGHRQVGVGFGSKGVLHTMWHVTRGAAIFIDNAVAGPYWADVKEDVVCYGGAWS 87
LIV NP_044677.1 1 SDLVYSGQGGQERGDRPFEVKDGVYRIFSPGLFWGQRQVGVGYGHKGVLHTMWHVTRGAALSIDDAVAGPYWADVKEDVVCYGGAWS 87
ALKV NC_004355.1 1 SELVFSGQGTRTERNRPFEIKDGAYRIYSPGLLWGHRQIGVGYGAKGVLHTMWHVTRGAALVVEEAISGPYWADVREDVVCYGGAWS 87
KFDV AFF18436.1 1 SELVFSGQETRTERNRPFEIKDGAYRIYSPGLLWGHRQIGVGYGAKGVLHTMWHVTRGAALVVDEAISGPYWADVREDVVCYGGAWS 87
POWV AAL32169.1 1 TDLVFSGQLSDHGEKRPFDIKDGVYRIYAPGLVWGHRQIGVGYGAKGVLHTMWHVTRGAALSVEGAVSGPYWADVREDVVCYGGAWS 87
YFV AAC72235.1 1 SGDVLWDIPTPKIIEECEHLEDGIYGIFQSTFL-GASQRGVGVAQGGVFHTMWHVTRGAFLVWNGKKLIPSWASVKEDLVAYGGSWK 86
WNV ABA62343.1 1 -GGVLWDTPSPKEYKKGD-TTTGVYRIMTRGLL-GSYQAGAGVMVEGVFHTLWHTTKGAALMSGEGRLDPYWGSVKEDRLCYGGPWK 84
KUNV AOS89779.1 1 -GGVLWDTPSPKEYKRGD-TTTGVYRIMTRGLL-GSYQAGAGVMVEGVFHTLWHTTKGAALMSGEGRLDPYWGSVKEDRLCYGGPWK 84
DENV-2 AEH59341.1 1 -AGVLWDVPSPPPVGKAE-LEDGAYRIKQKGIL-GYSQIGAGVYKEGTFHTMWHVTRGAVLMHKGKRIEPSWADVKKDLISYGGGWK 84
JEV ALI87293.1 1 -GGVFWDTPSPKPCSKGD-TTTGVYRIMARGIL-GTYQAGVGVMYENVFHTLWHTTRGAAIMSGEGKLTPYWGSVKEDRIAYGGPWR 84
ZIKV ANH10698.1 1 -SGALWDVPAPKEVKKGE-TTDGVYRVMTRRLL-GSTQVGVGVMQEGVFHTMWHVTKGSALRSGEGRLDPYWGDVKQDLVSYCGPWK 84
peptidase S7
TBM2
Accession:
90 100 110 120 130 140 150 160
TBEV AMP18887.1 88 LEEKWKG-ETVQVHAFPPGRAHEVHQCQPGELLLDTGRRIGAVPIDLAKGTSGSPILNSQGVVVGLYGNGLKT-NETYVSSIAQG-- 170
LGTV NP_620108.1 88 LESRWRG-ETVQVHAFPPGRAHETHQCQPGELILENGRKMGAIPIDLAKGTSGSPIMNSQGEVVGLYGNGLKT-NDTYVSSIAQG-- 170
OHFV NP_878909.1 88 LEEKWKG-EKVQVHAFPPGRAHEVHQCQPGELVLDTGRRIGAIPIDLAKGTSGSPILNAQGAVVGLYGNGLRT-NETYVSSIAQG-- 170
LIV NP_044677.1 88 LEEKWKG-ETVQVHAFPPGRAHEVHQCQPGELILDTGKRLGAIPIDLAKGTSGSPILNAQGVVVGLYGNGPKT-NESYVSSIAQG-- 170
ALKV NC_004355.1 88 LESRWRG-ETVQVHAFPPGRPQETHQCQPGELILENGRKLGAVPIDLSKGTSGSPIINAQGEVVGLYGNGLKT-NEAYVSSIAQG-- 170
KFDV AFF18436.1 88 LESRWRG-ETVQVHAFPPGRPQETHQCQPGELILENGRKLGAVPIDLSKGTSGSPIINAQGEVVGLYGNGLKT-NEAYVSSIAQG-- 170
POWV AAL32169.1 88 LEGKWGG-EVVQVHAFPPDSGHKVHQCQPGKLNLEGGRVMGAIPIDLPRGTSGSPIINAQGVVLGLYGNGLKS-NDVYISSIAQG-- 170
YFV AAC72235.1 87 LEGRWDGEEEVQLIAAAPGKNVVNVQTKPSLFKVRNGGEIGAVALDYPSGTSGSPIVNRNGEVIGLYGNGILVGDNSFVSAISQ--- 170
WNV ABA62343.1 85 LQHKWNGQDEVQMIVVEPGKNVKNVQTKPGVFKT-PEGEIGAVTLDFPTGTSGSPIVDKNGDVIGLYGNGVIMPNGSYISAIVQGER 170
KUNV AOS89779.1 85 LQHKWNGQDEVQMIVVEPGKNVKNVQTKPGVFKT-PEGEIGAVTLDFPTGTSGSPIVDKNGDVIGLYGNGVIMPNGSYISAIVQGER 170
DENV-2 AEH59341.1 85 LEGEWKEGEEVQVLALEPGKNPRAVQTKPGLFKT-NAGTIGAVSLDFSPGTSGSPIIDKKGKVVGLYGNGVVTRSGAYVSAIAQTEK 170
JEV ALI87293.1 85 FDRKWNGTDDVQVIVVEPGKAAVNIQTKPGVFRT-PFGEVGAVSLDYPRGTSGSPILDSNGDIIGLYGNGVELGDGSYVSAIVQGDR 170
ZIKV ANH10698.1 85 LDAAWDGHSEVQLLAVPPGERARNIQTLPGIFKT-KDGDIGAVALDYPAGTSGSPILDKCGRVIGLYGNGVVIKNGSYVSAITQGRR 170
B
HEK 293/ GFP
HEK 293/ TRAF6-GFP
GFP [α-GFP]
LGTV [α-NS3]
Merge/ DAPI
Inset
C
HEK 293
IgY
α-NS3
Mock
LGTV
Mock
LGTV
co-IP
TRAF6 [α-TRAF6]
NS3 [α-TBEV]
Input
TRAF6 [α-TRAF6]
NS3 [α-TBEV]
β-actin [α-β-actin]
D
HEK 293/ TRAF6-GFP
Mock
LGTV
KUNV
co-IP: TRAF6
NS3 [α-NS3]
TRAF6 [α-GFP]
Input
NS3 [α-NS3]
TRAF6 [α-GFP]
β-actin [α-β-actin]
E
NS2B/3
NS2B/3pro
NS3pro
NS5
TRAF6
Mock
NS2B/3 + TRAF6
TRAF6
NS2B/3
Mock
NS2B/3pro + TRAF6
TRAF6
NS2B/3pro
Mock
NS3pro + TRAF6
TRAF6
NS3pro
Mock
NS5 + TRAF6
TRAF6
NS5
Mock
TRAF6 + TRAF6
TRAF6
TRAF6
co-AP: TRAF6
POI [α-Mch]
TRAF6 [α-V5]
Input
POI [α-Mch]
TRAF6 [α-V5]
β-actin [α-β-actin]

Figure 1. LGTV NS3pro Interacts with TRAF6

(A) Sequence alignment of tick- or mosquito-borne flavivirus NS3pro. Putative TBMs are underlined, and anchor amino acids are highlighted in blue. Conserved residues of the catalytic triad are highlighted in red.

(B) Representative images of colocalization of LGTV NS3 and TRAF6. HEK293 cells expressing GFP or TRAF6-GFP were infected with LGTV at an MOI of 1. Cells were processed at 24 hpi, stained with anti-NS3 (red) and anti-GFP (green) antibodies, and visualized by confocal microscopy. Nuclei were stained with DAPI (blue); scale bar (white solid line), 10 μM. Yellow represents co-localized proteins. White box indicates area of enlargement in inset panel; inset scale bar (white solid line), 5 μM. White arrowhead indicates a distinct TRAF6 punctum observed in uninfected cells.

(C) CoIP of LGTV NS3 and endogenous TRAF6 during infection. HEK293 cells were infected with LGTV at an MOI of 1. Cell lysates were prepared at 48 hpi, incubated with either anti-NS3 or control IgY antisera, and precipitated with PrecipHen beads. Samples were analyzed by immunoblot with the indicated antibodies. Results representative of two independent experiments.

(D) CoIP of LGTV NS3 and TRAF6. HEK293 cells expressing TRAF6-GFP were infected with LGTV or KUNV at an MOI of 10. Cell lysates were immunoprecipitated with anti-GFP antibody and protein-A-conjugated agarose beads at 48 hpi. Samples were analyzed by immunoblot with the indicated antibodies. Results representative of three independent experiments.

(E) CoAP of recombinant LGTV NS3 constructs with TRAF6. HEK293 cells were transfected with 2 μg of each indicated plasmid. Cell lysates were pulled down using streptavidin-conjugated beads at 24 h post-transfection, and eluted proteins were analyzed by immunoblot with indicated antibodies. Results representative of three or more independent experiments. POI, protein of interest.

See also Figure S1.

ubiquitin ligase and binds substrate proteins through a conserved TRAF6 binding motif (TBM). A canonical TBM is formed from the amino acid sequence P-X-E-X-X-Ac/Ar (X representing any amino acid, Ac/Ar representing either an acidic or aromatic residue) (Chung et al., 2007). TRAF6 has also been shown to bind to non-canonical TBMs that have alternative amino acids sequences (Gentry et al., 2004; Meads et al., 2010; Noels et al., 2007; Stack et al., 2013).

In this study, we discovered and experimentally validated a TBM in NS3 of tick-borne flaviviruses (TBFVs), which is not present in mosquito-borne flaviviruses (MBFVs). The protein interaction between TRAF6 and NS3 is disrupted by site-directed mutagenesis, and, in the context of the full TBFV genome, the mutation results in virus attenuation. We found that TBM mutation within NS3 impairs the expression of the mature, active form of the viral protease (NS3pro). NS3pro is only produced during infection by autoproteolytic cleavage and is essential for flavivirus replication. Our data suggest that TRAF6 actively participates in the TBFV replication cycle to maintain NS3pro expression, possibly through protein stabilization or protease activation. Thus TRAF6's structural and functional contributions to NS3pro maturation, in addition to the TRAF6-NS3 complex, serve as potential therapeutic targets that should be further explored for treatment of the TBFVs.

RESULTS

TBFV, but Not MBFV, NS3pro Interacts with TRAF6

To investigate the cellular factors regulating TBFV replication, we performed a bioinformatic analysis of the TBEV polyprotein using the Eukaryotic Linear Motif Resource for Functional Sites in Proteins (Dinkel et al., 2013). Our primary screen revealed a solitary putative canonical TBM, P-F-E-V-K-D (TBM1), located within the protease domain of NS3 (NS3pro) between residues 17 and 22 (Figure 1A). Further analysis of NS3pro identified a non-canonical putative TBM, P-G-E-L-L-L (TBM2), at residues 115–120, in which the terminal amino acid of the consensus sequence is neither acidic nor aromatic (Figure 1A) (Gentry et al., 2004). Sequence alignment of NS3pro from other flaviviruses showed that the two putative TBMs are highly conserved among TBFVs (Figures 1A and S1A–S1C), with the exception of the evolutionarily isolated POWV (Hermance and Thangamani, 2017). TBM2 was not present in NS3 of POWV. Furthermore, we did not identify TBM1 or TBM2 in any MBFV (Figure 1A), suggesting a possible unique and specific interaction between TBFVs and TRAF6.

Based on our bioinformatics results, we first examined a potential interaction between TBFV NS3 and TRAF6 using immunofluorescent microscopy. For this purpose, human embryonic kidney (HEK) 293 cells expressing either GFP or a GFP-tagged TRAF6 (TRAF6-GFP) were infected with Langat virus (LGTV), a prototypical member of the TBEV serogroup. Confocal analyses revealed strong co-localization of LGTV NS3 and TRAF6 proteins at 24 h post-infection (hpi) (Figure 1B). We also observed a change in the cellular distribution of TRAF6-GFP, from discrete puncta in uninfected cells to a large perinuclear aggregate during infection (Figure 1B). To validate the confocal results, we took a biochemical approach and preformed a co-immunoprecipitation (coIP) of endogenous TRAF6 with LGTV NS3. HEK293 cells were infected with LGTV, and at 48 hpi, anti-NS3 antibody was used to precipitate LGTV NS3. We were able to pull down

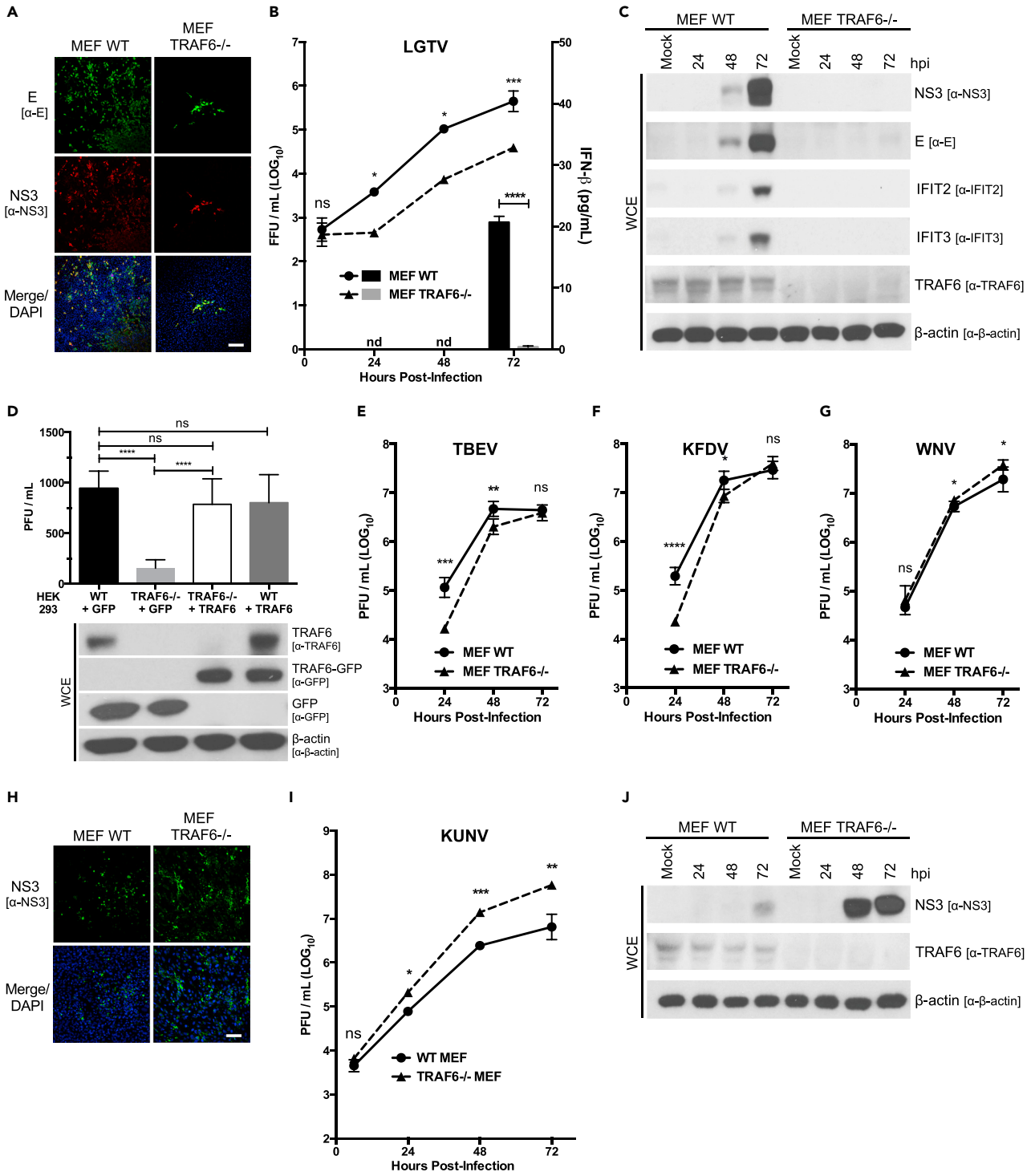

Figure 2. TRAF6 Is a Proviral Factor for TBFVs

(A) Representative images of confocal microscopy of LGTV-infected WT or TRAF6$^{-/-}$ MEFs. MEFs were infected at an MOI of 1 and were processed at 24 hpi. Cells were immunostained with anti-E (green) and anti-NS3 (red) antibodies. Nuclei were stained with DAPI (blue); scale bar (white solid line), 200 μM.

(B) Titration of infectious particles in the supernatant from WT or TRAF6$^{-/-}$ MEFs infected with LGTV (MOI of 0.1) for indicated times (h). Viral titers were determined by immunofocus assay (left y axis). IFN-β protein in supernatants from infected cells was quantitated by ELISA and is represented by a column graph (right y axis). Results are representative of three or more independent experiments performed in triplicate and plotted as mean ± SEM. ns, not significant; *p < 0.05, ***p < 0.001.

Figure 2. *Continued*

(C) Immunoblot analysis of whole-cell extracts from WT or TRAF6$^{-/-}$ MEFs infected with LGTV (MOI 0.1) for indicated times (h). Blots were probed with antibodies to LGTV NS3, LGTV E, IFIT2, IFIT3, TRAF6, and β-actin. Results representative of three or more independent experiments. See Figure S2A for longer exposures of LGTV NS3 and LGTV E.

(D) Titration of infectious particles in the supernatant from WT or TRAF6$^{-/-}$ HEK293 cells expressing either GFP or TRAF6-GFP infected with LGTV (MOI of 0.1) at 24 hpi. Viral titers were determined by plaque assay. Whole-cell extracts from the infected cells were analyzed by immunoblot using GFP, TRAF6, and β-actin antibodies. Data are average of three independent experiments performed in triplicate and plotted as mean ± SEM. ns, not significant; ****$p < 0.0001$.

(E–G) Titration of infectious particles in the supernatant from WT or TRAF6$^{-/-}$ MEFs infected with TBEV (E), KFDV (F), or WNV (G) (MOI of 0.1) for indicated times (h). Viral titers were determined by plaque assay. Data are average of three independent experiments performed in triplicate and plotted as mean ± SEM. ns, not significant; *$p < 0.05$, **$p < 0.01$, ***$p < 0.001$, ****$p < 0.0001$.

(H) Representative images of confocal microscopy of KUNV-infected WT or TRAF6$^{-/-}$ MEFs. MEFs were infected at an MOI of 1 and were processed at 24 hpi. Cells were immunostained with anti-NS3 (green) antibodies. Nuclei were stained with DAPI (blue); scale bar (white solid line), 100 μM.

(I) Titration of infectious particles in the supernatant from WT or TRAF6$^{-/-}$ MEFs infected with KUNV (MOI of 0.1) for indicated times (h). Viral titers were determined by plaque assay. Data are representative of three or more independent experiments performed in triplicate and plotted as mean ± SEM. ns, not significant; *$p < 0.05$; **$p < 0.01$; ***$p < 0.001$.

(J) Immunoblot analysis of whole-cell extracts from WT or TRAF6$^{-/-}$ MEFs infected with KUNV (MOI 0.1) for indicated times (h). Blots were probed with antibodies to WNV NS3, TRAF6, and β-actin. Results representative of three or more independent experiments.

See also Figure S2.

endogenous TRAF6 with LGTV NS3 (Figure 1C). In addition, we tested the specificity of TBFV NS3 to interact with TRAF6 by preforming a coIP with HEK293 cells expressing TRAF6-GFP. Cells were either infected with LGTV or Kunjin virus (KUNV), an MBFV that lacks TBM1 and TBM2 (Figure 1A), and at 48 hpi, anti-GFP antibody was used to precipitate TRAF6-GFP. We were only able to pull down LGTV NS3 with TRAF6-GFP (Figure 1D). These results suggest that LGTV NS3 and TRAF6 proteins interact during TBFV infection.

To identify the structural and functional requirements of the LGTV NS3pro-TRAF6 interaction, we engineered epitope-tagged recombinant NS3 constructs and compared their interaction with wild-type (WT) TRAF6 using a co-affinity purification (coAP) technique based on biotin-streptavidin binding (Taylor et al., 2011). NS3 protease activity is dependent on a non-covalent interaction with NS2B (Erbel et al., 2006; Falgout et al., 1991). To express NS3 with a functional protease domain, we fused NS2B and NS3 together in a single open reading frame, as occurs in the polyprotein (NS2B/3). Once translated within the cell, the NS2B/3 polyprotein undergoes autocatalytic cleavage, freeing NS2B from NS3 (Bera et al., 2007; Liu et al., 2017). This cleavage event is detected on immunoblot as a doublet, with NS2B/3 having a larger molecular weight than NS3 alone. As a confirmation of the interaction detected during virus infection, TRAF6 precipitated both full-length LGTV NS2B/3 and truncated LGTV NS2B/3pro when expressed in HEK293 cells (Figure 1E). Next, we engineered the following two constructs to directly test the requirement of NS3 protease activity for NS3pro binding to TRAF6: (1) an LGTV NS3pro construct that lacks NS2B and thus has no enzymatic activity and (2) a mutated LGTV NS3 serine 138 to alanine, which disrupts the catalytic triad needed for protease activity (Pastorino et al., 2006). We found in both instances that NS3 was able to interact with TRAF6 regardless of a functional NS3 protease (Figures 1E, S1D, and S1E). Finally, LGTV NS5, the major interferon (IFN) antagonist of TBFVs (Best et al., 2005), was not precipitated with TRAF6 and served as a negative control, whereas TRAF6 forms a strong homomeric complex with alternatively tagged TRAF6 as previously reported (Megas et al., 2011) (Figure 1E). These results show that TRAF6 specifically interacts with the protease domain of LGTV NS3 and that the protease activity of NS3 is not required for this interaction.

TBFVs Use TRAF6 for Optimal Replication

To assess the role of TRAF6 in TBFV replication, we infected WT and TRAF6$^{-/-}$ murine embryonic fibroblasts (MEFs) with LGTV. In contrast to what we predicted, we found that TRAF6 is needed for optimal LGTV replication (Figures 2A–2C and S2A). There was up to a 14.2-fold reduction in the release of infectious virions from TRAF6-deficient cells compared with cells expressing TRAF6 (Figure 2B). Moreover, NS3 and E proteins were readily detectable in LGTV-infected WT MEFs compared with TRAF6$^{-/-}$ MEFs (Figures 2C and S2A). We observed a similar reduction in LGTV replication when we infected CRISPR/Cas9-generated TRAF6$^{-/-}$ HEK293 cells (Figure S2B). To demonstrate that the reduction in LGTV titers was due to a lack of TRAF6, we complemented TRAF6$^{-/-}$ HEK293 cells with human TRAF6-GFP and found that LGTV titers were restored to WT levels (Figure 2D). In addition, we functionally depleted HEK293 cells of TRAF6 using a commercially available TRAF6 peptide inhibitor (Hou et al., 2014) and by overexpressing a TRAF6 construct

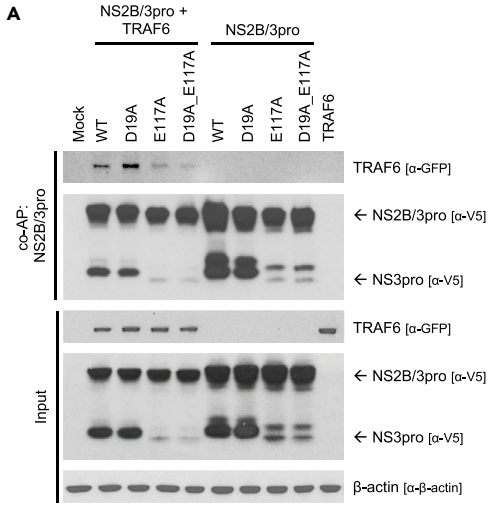

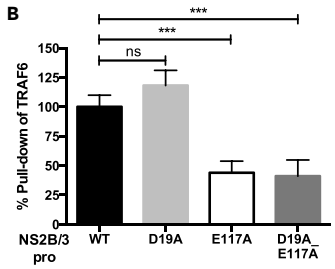

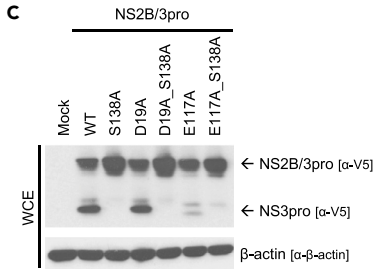

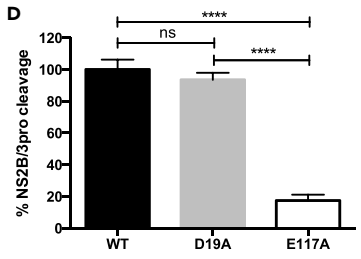

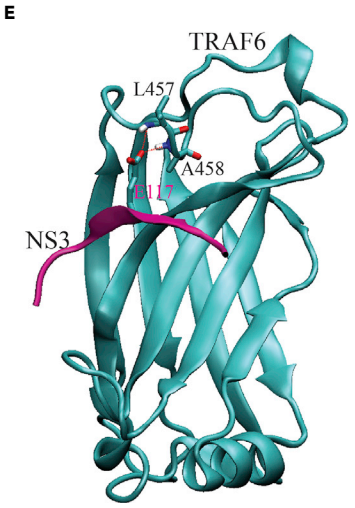

Figure 3. An E117A Mutation in LGTV NS3pro Disrupts TRAF6 Binding and Mature Protease Accumulation

(A) CoAP of mutant LGTV NS2B/3pro constructs with TRAF6. HEK293 cells were transfected with 2 μg of each indicated plasmid. Cell lysates were pulled down using streptavidin-conjugated beads at 24 h post-transfection, and eluted proteins were analyzed by immunoblot with indicated antibodies. Results representative of three independent experiments.

(B) Quantification of TRAF6 pull-down by mutant LGTV NS2B/3pro constructs in (A). Precipitated TRAF6-GFP from three independent experiments were quantitated using ImageJ after normalization to β-actin. Data are presented as percent pull-down of TRAF6-GFP relative to NS2B/3pro WT ± SD. ns, not significant; ***$p < 0.001$.

(C) Immunoblot analysis of whole-cell extracts from HEK293 cells expressing mutant LGTV NS2B/3pro constructs. HEK293 cells were transfected with 2 μg of each indicated plasmid and processed 24 h post-transfection. Blots were probed with indicated antibodies. Results representative of three independent experiments.

Figure 3. *Continued*

(D) Quantification of cleaved NS3pro of mutant LGTV NS2B/3pro constructs in (C). Cleaved NS3pro from three independent experiments were quantitated using ImageJ after normalization to β-actin. Data are presented as percent cleavage relative to NS2B/3pro WT ± SD. ns, not significant; ****$p < 0.0001$.

(E) The modeled structure of the complex of the LGTV NS3pro TBM2 (colored in magenta) with the C-terminal MATH domain of TRAF6 (colored in cyan). Dashed lines indicate dual hydrogen bonds between the omega oxygen atom of E117 of NS3 and the backbone amide N-H groups of L457 and A458 of TRAF6.

See also Figure S3.

with a mutation in the ligase catalytic site (Ning et al., 2008). In both cases, LGTV replication was significantly diminished to levels similar to TRAF6$^{-/-}$ cells (Figures S2C–S2E). Conversely, LGTV replication was similar between TRAF6-GFP overexpressing cells and control cells, suggesting that endogenous TRAF6 is sufficient for the observed proviral effect during LGTV infection (Figures 2D, S2D, and S2E). Furthermore, we infected TRAF6$^{-/-}$ cells with the highly virulent TBEV and KFDV and observed similar trends as with LGTV (Figures 2E, 2F, S2F, and S2G). There was a 9.9-fold reduction in TBEV and 8.6-fold reduction in KFDV titers in TRAF6$^{-/-}$ MEFs at 24 hpi (Figures 2E and 2F), suggesting that TRAF6 promotes the replication of TBFVs regardless of their virulence.

To assess the interplay between TBFV replication, TRAF6, and IFN production, we quantified IFN-β in the supernatant of LGTV-infected TRAF6$^{-/-}$ MEFs. We were only able to detect IFN-β (20.6 pg/mL) at 72 hpi in the supernatant from WT MEFs. IFN-β remained undetectable in the supernatants from TRAF6$^{-/-}$ MEFs throughout the course of infection (Figure 2B). Moreover, the levels of IFN-β directly correlated with the expression of the IFN-stimulated genes, IFIT2 and IFIT3, as detected by immunoblot of the cell lysates (Figure 2C). These data indicate that the attenuation of LGTV replication in TRAF6$^{-/-}$ MEFs is not due to increased IFN production.

To compare the impact of TRAF6 on TBFVs to MBFVs, we infected TRAF6$^{-/-}$ MEFs with WNV and KUNV. We observed a striking difference between the MBFVs and TBFVs (Figures 2G–2J). The replication of WNV and KUNV was enhanced in the absence of TRAF6, both reaching higher viral titers in MEFs deficient in TRAF6 compared with WT (Figures 2G and 2I). Infection of TRAF6$^{-/-}$ MEFs resulted in up to 8.9-fold increase in KUNV titers and an increase in NS3 production compared with WT MEFs (Figures 2H–2J). Taken together, these results show that TRAF6 specifically supports TBFV replication, which is distinctly different from its antiviral role in MBFV infection.

Mutation of TBM2 Prevents TRAF6-NS3pro Interaction and Reduces Accumulation of the Mature Protease

Previous studies have shown that mutation of the anchor glutamic acid residue in a TBM to an alanine disrupts TRAF6 binding (Verstak et al., 2014; Yu et al., 2016). To determine which TBM(s) in LGTV NS3pro interacts with TRAF6, we mutated the acidic amino acid in each TBM of LGTV NS2B/3pro to alanine. We tested the ability of each mutant to bind TRAF6 by coAP assay. We found that a D19A mutation in TBM1 had no effect on binding, whereas an E117A mutation in TBM2 resulted in a significant decrease in binding to TRAF6 (Figure 3A). E117A mutation also diminished the TRAF6 interaction to NS2B/3pro_D19A mutant (Figure 3A). Quantification of immunoblots using densitometry showed a 56.1% and a 58.6% decrease in pull down of TRAF6 by LGTV NS2B/3pro_E117A and LGTV NS2B/3pro_D19A_E117A, respectively (Figure 3B).

After performing coAP assays with LGTV NS2B/3pro mutants, we noticed that constructs with an E117A mutation had reduced levels of the cleaved, mature form of NS2B/3pro (Figure 3A). The disappearance of NS3pro could be due to a structural change in protein stability, or a functional change in protease activity leading to decreased autoproteolytic cleavage. To confirm that the lower-molecular-weight protein was produced by autocatalytic cleavage, we inactivated the protease by an additional S138A mutation, which resulted in a total loss of the lower molecular weight band (Figure 3C). Quantification of immunoblots by densitometry showed that the E117A mutation reduced mature NS3pro accumulation by 82.5% compared with the WT or D19A proteins (Figure 3D).

To further assess the TRAF6-NS3pro interaction at TBM2, we modeled the interaction of LGTV NS3pro and TRAF6 *in silico*. The crystal structures of TRAF6 and substrate ligands have been solved for several complexes and demonstrate a specific pattern of hydrogen bonding between the MATH domain of TRAF6

Intermolecular Pair	ΔE^{gas} (kcal/mol)	$\Delta E^{solution}$ (kcal/mol)
E117 of NS3 — L457, A458 of TRAF6	−19.23	−3.60
A117 of NS3 — L457, A458 of TRAF6	−0.09	−0.16

Table 1. Intermolecular Interaction Energies between E117 or A117 of LGTV NS3pro and the Backbone Amide N-H Groups of L457 and A458 of TRAF6

ΔE^{gas} and $\Delta E^{solution}$ represent intermolecular interaction energy in vacuum and in aqueous solution, respectively. Intermolecular interaction energies were calculated with the supermolecular approach at the MP2/6-311++G** level.
See also Figure S3.

and the TBM of an interacting protein (Shi et al., 2015; Ye et al., 2002). Indeed, it was from these structures and through mutational analysis that the canonical TBM was determined. We set out to use these data to evaluate the structural interaction of LGTV NS3pro and TRAF6 through TBM2. Unfortunately, no crystal structure exists for any TBFV NS3. So, we began by first generating an LGTV NS3pro model using homology modeling with Murray Valley encephalitis virus NS3 crystal structure as a template (Assenberg et al., 2009) (Figure S3A). TBM2 of LGTV NS3pro was found to form a beta strand that is situated on the surface of the protein (Figure S3B). Next, we modeled the structure of the complex of the TBM2 of LGTV NS3pro with the MATH domain of TRAF6 (Figure 3E). The negatively charged omega oxygen atom of E117 of LGTV NS3 formed dual hydrogen bonds with the backbone amide N-H groups of L457 and A458 of TRAF6 (Figure 3E). The intermolecular interaction energies between E117 of LGTV NS3pro and their interacting protein partners in TRAF6 were calculated at the MP2/6-311++G** level using the supermolecular approach with the Gaussian 09 package (Frisch et al., 2009) as described previously (Mao et al., 2003). The resulting interaction energies in both the gas phase (ΔE^{gas}) and the solution phase ($\Delta E^{solution}$) are listed in Table 1. For comparison, the calculated intermolecular interaction energies between the mutated A117 residue of LGTV NS3 and their interacting protein partners are also listed. In the NS3pro_E117A mutant, the dual hydrogen bonds are lost, which results in a binding energy loss of 3.44 kcal/mol in the solution phase. Overall, both *in silico* and biological data support the conclusion that an E117A mutation in NS3pro interferes with TRAF6 binding. The unexpected result of the E117A mutation on the abundance of mature NS3pro warrants further studies into the potential effect(s) of TRAF6 on NS3pro structure and protease function.

An LGTV Mutant Virus Containing the E117A Mutation Exhibits a Small Plaque Phenotype and Is Attenuated In Vitro

To test the impact of an E117A mutation on the ability of LGTV to replicate, we created the mutation in the LGTV infectious clone. The plaque-forming ability of the LGTV NS3_E117A mutant was noticeably reduced compared with that of the LGTV following transfection of equal amounts of *in vitro* transcribed mRNA (Figure 4A). Also, recovered LGTV NS3_E117A foci were reduced by 81.8% compared with recovered WT and NS3_D19A LGTV (Figure 4B). Consistently, we observed reduced replication of LGTV NS3_E117A in HEK293 cells compared with LGTV and LGTV NS3_D19A by immunofluorescent microscopy, immunofocus assay, and immunoblotting (Figures 4C–4E). There was up to a 17.4-fold reduction in the release of infectious virions from LGTV NS3_E117A-infected cells compared with cells infected with LGTV or LGTV NS3_D19A (Figure 3D). To test if LGTV NS3_E117A attenuation is due to an impaired ability to co-opt TRAF6 during replication, we infected WT and TRAF6$^{-/-}$ MEFs with LGTV NS3_E117A and LGTV. Similar to observations made with HEK293 cells, replication of LGTV NS3_E117A was reduced by 7.8-fold compared with LGTV in WT MEFs (Figure 4F). Alternatively, the attenuation of LGTV NS3_E117A was lost in TRAF6$^{-/-}$ MEFs; there was no statistical difference between titers from LGTV NS3_E117A and LGTV-infected TRAF6$^{-/-}$ MEFs (Figure 4F). Taken together, these data suggest that an E117A mutation in NS3 impairs LGTV replication and that this attenuation is dependent on TRAF6.

DISCUSSION

In this study, we provide evidence that TRAF6 plays an unexpected proviral role in TBFV replication. We found that TRAF6 interacts with TBFV NS3pro in a sequence-dependent manner and that targeted inhibition of the complex formation leads to virus attenuation.

We have identified a non-canonical TBM that appears to be conserved among closely related TBFVs and is not present in MBFVs (Figure 1A). A physical interaction between flavivirus NS3 and TRAF6 has not been previously reported. It has been shown that NS3 from classical swine fever virus (CSFV), a pestivirus, binds

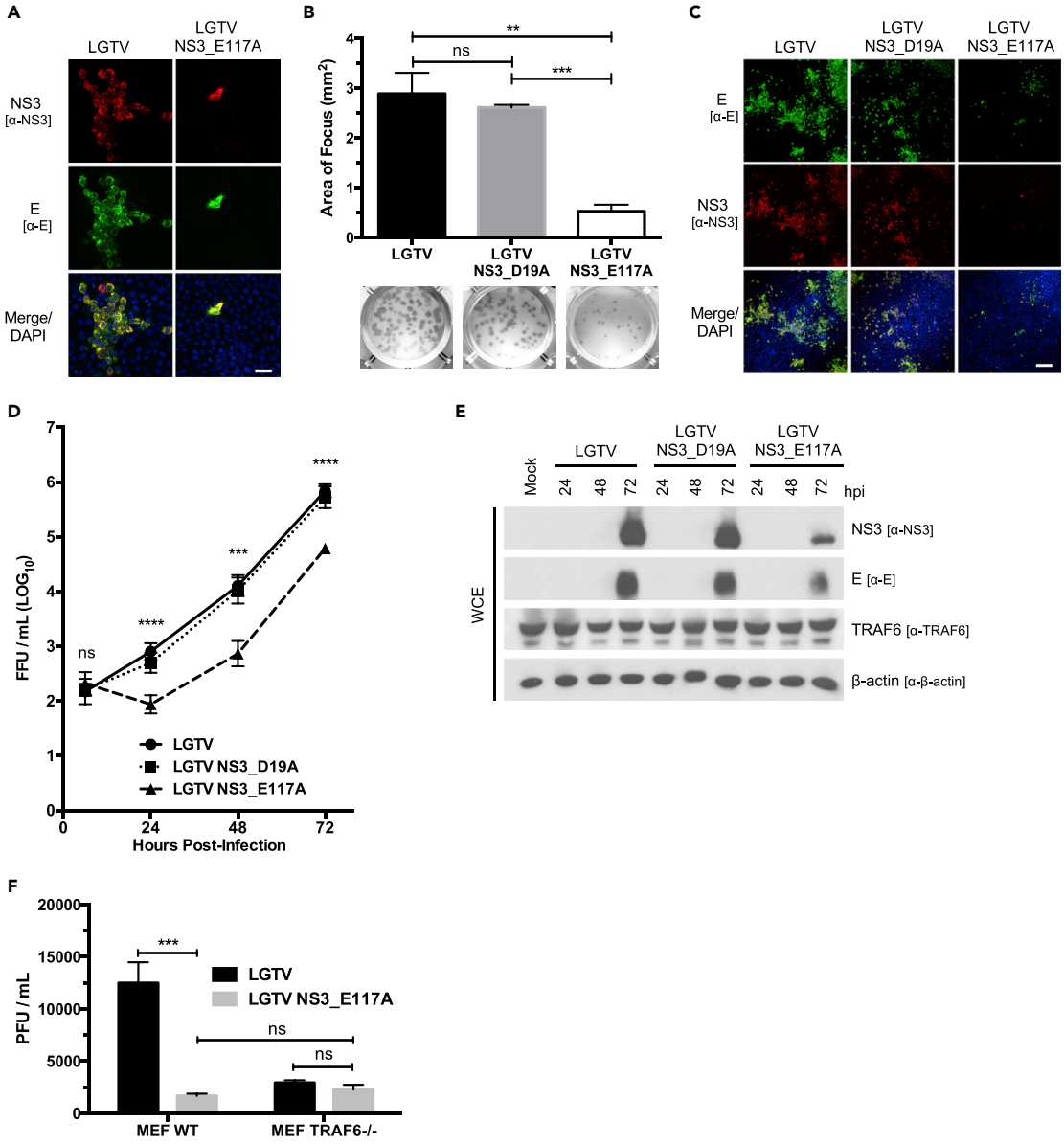

Figure 4. LGTV NS3 E117A Mutant Virus Is Attenuated *In Vitro*

(A) Representative images of confocal microscopy of HEK293 cells transfected with either LGTV or LGTV_E117A *in vitro*-transcribed genomic RNA. Cells were processed at 72 h post-transfection and immunostained with anti-NS3 (red) and anti-E (green) antibodies. Nuclei were stained with DAPI (blue); scale bar (white solid line), 50 μM.

(B) Measurement of viral foci in Vero cells infected with recovered LGTV, LGTV NS3_D19A, or LGTV NS3_E117A. The area (mm^2) of individual foci formed by each virus was calculated using ImageJ. Representative foci of each virus are presented below the column graph. Data are average of three independent experiments performed in triplicate and plotted as mean ± SEM. ns, not significant; **$p < 0.01$; ***$p < 0.001$.

(C) Representative images of confocal microscopy of HEK293 cells infected with LGTV, LGTV NS3_D19A, or LGTV NS3_E117A. HEK293 cells were infected at an MOI of 0.1 and were processed at 24 hpi. Cells were immunostained with anti-E (green) and anti-NS3 (red) antibodies. Nuclei were stained with DAPI (blue); scale bar (white solid line), 200 μM.

(D) Titration of infectious particles in the supernatant from HEK293 cells infected with LGTV, LGTV NS3_D19A, or LGTV NS3_E117A (MOI of 0.1) for indicated times (h). Viral titers were determined by immunofocus assay. Data are representative of three or more independent experiments performed in triplicate and plotted as mean ± SEM. ns, not significant; ***$p < 0.001$; ****$p < 0.0001$.

(E) Immunoblot analysis of whole-cell extracts from HEK293 cells infected with LGTV, LGTV NS3_D19A, or LGTV NS3_E117A (MOI 0.1) for indicated times (h). Blots were probed with antibodies to LGTV NS3, LGTV E, TRAF6, and β-actin. Results representative of three or more independent experiments.

Figure 4. *Continued*

(F) Titration of infectious particles in the supernatant from WT or TRAF6$^{-/-}$ MEFs infected with LGTV or LGTV NS3_E117A (MOI of 0.1) at 24 hpi. Viral titers were determined by plaque assay. Data are representative of three independent experiments performed in triplicate and plotted as mean ± SEM. ns, not significant; ***$p < 0.001$.

and degrades TRAF6 to prevent activation of NF-κB signaling pathways during infection (Lv et al., 2017). Although CSFV is a member of the Flaviviridae, it differs from flaviviruses in several ways. (1) The genome of CSFV is composed of a different number and set of genes than flaviviruses (Tautz et al., 2015); (2) CSFV NS3 requires NS4A, not NS2B, as an essential cofactor of protease activity (Tautz et al., 2000); (3) CSFV is not transmitted by arthropod vectors; and (4) CSFV does not cause disease in humans (Blome et al., 2017).

TRAF6 is conventionally associated with host innate immune protection because of its pivotal role in IL-1/TLR and RIG-I signaling (Inoue et al., 2007; Yoshida et al., 2008). It was previously shown that prototypical RNA viruses replicate better and are more cytopathic in TRAF6-deficient cells because of a mitigated IFN response (Konno et al., 2009; Yoshida et al., 2008). Studies examining the role of TRAF6 during flavivirus infection have been limited to MBFVs. DENV and Japanese encephalitis virus (JEV) have been found to up-regulate cellular miR-146a to decrease expression and signaling of TRAF6; suppression of TRAF6 leads to decreased NF-κB activation, Jak-STAT signaling, and IFN production, and in the case of DENV, also inhibited virus-induced autophagy (Pu et al., 2017; Sharma and Verma, 2015; Wu et al., 2013). The effect of TBFV NS3 binding to TRAF6 is an intriguing and unexplored question for follow-up studies, especially if TBFV NS3 binding to TRAF6 inhibits the canonical antiviral signaling role for TRAF6, while using TRAF6 to benefit virus replication.

It was unexpected when we observed better replication of TBFVs in WT MEFs compared with TRAF6$^{-/-}$ MEFs (Figures 2A–2C, 2E, and 2F). Indeed, because our findings differ from precedent, we took multiple approaches to validate the proviral effects of TRAF6 in TBFV infection. (1) We used two independently generated TRAF6 knockout cell lines: embryonically derived TRAF6$^{-/-}$ MEFs and CRISPR/Cas9 generated TRAF6$^{-/-}$ HEK293 cells (Figures 2A–2C and S2B). (2) We functionally depleted WT cells of TRAF6 by overexpressing an enzymatically inactive TRAF6 mutant (Figures S2D and S2E). (3) We treated WT cells with a TRAF6 inhibitor peptide (Figure S2C). (4) We mutated TBM2 within a TBFV genome (Figure 4). Under all these conditions, we consistently saw TBFV attenuation. Furthermore, the phenotype could be rescued by the expression of TRAF6 (Figure 2D).

When we assessed MBFV replication in our TRAF6$^{-/-}$ MEFs, using WNV and KUNV, we observed a reciprocal phenotype than what was seen with TBFVs. MBFV replication was enhanced in the absence of TRAF6, similar to previous DENV and JEV studies (Figures 2G–2J). As predicted from our sequence analysis (Figure 1A), KUNV NS3 did not interact with TRAF6 during infection (Figure 1D). Furthermore, we saw better LGTV replication in WT MEFs compared with TRAF6$^{-/-}$ MEFs despite higher IFN-β production (Figure 2B). Taken all together, our findings demonstrate that the proviral function of TRAF6 is specific to TBFVs.

An E117A mutation in TBM2 of NS3pro revealed that interaction with TRAF6 is needed for the accumulation of the mature processed form of the protease. Note that TRAF6-NS3pro binding is not essential for protein function. This allowed us to design and recover mutant LGTV NS3_E117A, which was attenuated to similar levels seen with WT LGTV in TRAF6-deficient cells (Figures 4D and S2B). We failed to precipitate TRAF6 from LGTV NS3_E117A-infected cells (data not shown); these experiments were confounded by reduced viral protein levels associated with the LGTV NS3_E117A (Figure 4E). LGTV NS3_E117A attenuation is most likely a result of decreased interaction with TRAF6 because the difference between mutant and WT virus is lost in TRAF6$^{-/-}$ MEFs (Figure 4F). In contrast, overexpression of TRAF6 did not enhance virus production, suggesting that the endogenous level of TRAF6 is sufficient for optimal virus replication (Figures 2D and S2D), albeit viral protein levels were modestly elevated (Figure S2E).

We are currently evaluating how TRAF6 benefits TBFV replication, looking specifically for structural changes to NS3pro when complexed with TRAF6 and changes to overall protease activity. TRAF6 is an E3 ubiquitin ligase and performs its normal physiological function by ubiquitinating itself and substrate proteins (Walsh et al., 2015). TBFV NS3pro may be modified by TRAF6-mediated non-degradative ubiquitination; this hypothesis is supported by our observation of LGTV attenuation in cells overexpressing an enzymatically inactive TRAF6 (Figures S2D and S2E). It has previously been shown that K27-linked ubiquitination of DENV NS3 facilitates NS2B recruitment and NS2B/3pro complex formation; the ligase has yet to be identified (Liu et al., 2017).

The flavivirus NS3 is an attractive therapeutic target because it is essential for virus replication and has well-characterized enzymatic functions (Leyssen et al., 2000). Substantial effort and resources have been put into the design of inhibitors of NS3pro activity, but there has only been limited success and no compound has reached the clinical trial stage. It has been challenging to develop NS3pro inhibitors because the active site is shallow and highly charged (Luo et al., 2015). We propose that the TRAF6-NS3pro interaction may serve as an antiviral target. Specific disruption of the TRAF6-NS3pro complex, as demonstrated by our use of a TRAF6 inhibitor peptide in this study (Figure S2C), could indirectly inhibit NS3 function and be accomplished without having to overcome the multiple obstacles that are associated with development of compounds that directly inactivate NS3. Likewise, we speculate that the attenuation and small plaque phenotype of the E117A mutant virus *in vitro* may result in impaired *in vivo* pathogenesis as reported for other mutant flaviviruses, including LGTV (Blaney et al., 2002; Eastman and Blair, 1985; Hanley et al., 2002; Rumyantsev et al., 2006).

Overall, our study demonstrates that specific flavivirus therapeutic targets may be identified by first understanding how viruses and host cell proteins interact. By identifying a specific interaction between TRAF6 and TBFV NS3pro, we revealed a mechanism used by viruses to co-opt host cell antiviral molecules for viral gain.

Limitations of the Study

There are still many issues to be investigated regarding the role of TRAF6 in TBEV infection, including (1) the exact mechanism as to how a TRAF6-NS3pro interaction affects mature NS3pro accumulation and ultimately virus replication; TRAF6, a E3 ubiquitin ligase, may ubiquitinate NS3 directly or act as a scaffold protein bring together other host or viral proteins; and (2) the importance of TRAF6 in TBFV pathogenesis in primary cells, including dendritic cells and neurons, and within *in vivo* models. (3) Our investigations only examine the proviral role of TRAF6 in TBFV infection; however, TBFV antagonism of the antiviral activity of TRAF6 likely contributes to the overall success of TBFVs to cause disease.

METHODS

All methods can be found in the accompanying Transparent Methods supplemental file.

SUPPLEMENTAL INFORMATION

Supplemental Information can be found online at https://doi.org/10.1016/j.isci.2019.05.010.

ACKNOWLEDGMENTS

We thank Drs. Malathi Krishnamurthy, R. Mark Wooten, and Stanislaw Stepkowski for their guidance and intellectual contributions in helping shape the overarching direction of research. We also thank Dr. Jyl S. Matson for the use of her plate reader and Dr. Alexander G. Pletnev for providing the LGTV infectious clone. We are pleased to acknowledge the Ohio Supercomputer Center for a generous allocation of supercomputer time. This work was supported in part by the Intramural Research Program of the National Institutes of Health and National Institute of Allergy and Infectious Diseases: ZIA-AI001125 to S.M.B. and 1K22-AI099020 to R.T.T.

AUTHOR CONTRIBUTIONS

Conceptualization, B.H.Y., S.M.B., and R.T.T.; Methodology, B.H.Y., S.A., X. H., and R.T.T.; Formal Analysis, B.H.Y., S.A., X. H., and R.T.T.; Investigation, B.H.Y., T.G.B., K.L.M., A.O.I., K.J.L., J.B.P., S.A., X.H., and R.T.T.; Writing – Original Draft, B.H.Y. and R.T.T.; Writing – Review & Editing, B.H.Y., S.M.B., S.C., X.H., and R.T.T.; Funding Acquisition, S.M.B. and R.T.T.; Resources, S.C., S.M.B., X.H., and R.T.T.; Visualization, B.H.Y. and R.T.T.; Supervision, R.T.T.

DECLARATION OF INTERESTS

The authors declare no competing interests.

Received: November 2, 2018
Revised: January 18, 2019
Accepted: May 8, 2019
Published: May 31, 2019

REFERENCES

Assenberg, R., Mastrangelo, E., Walter, T.S., Verma, A., Milani, M., Owens, R.J., Stuart, D.I., Grimes, J.M., and Mancini, E.J. (2009). Crystal structure of a novel conformational state of the flavivirus NS3 protein: implications for polyprotein processing and viral replication. J. Virol. *83*, 12895–12906.

Bera, A.K., Kuhn, R.J., and Smith, J.L. (2007). Functional characterization of cis and transActivity of the flavivirus NS2B-NS3 protease. J. Biol. Chem. *282*, 12883–12892.

Best, S.M., Morris, K.L., Shannon, J.G., Robertson, S.J., Mitzel, D.N., Park, G.S., Boer, E., Wolfinbarger, J.B., and Bloom, M.E. (2005). Inhibition of interferon-stimulated JAK-STAT signaling by a tick-borne flavivirus and identification of NS5 as an interferon antagonist. J. Virol. *79*, 12828–12839.

Blaney, J.E., Jr., Johnson, D.H., Manipon, G.G., Firestone, C.-Y., Hanson, C.T., Murphy, B.R., and Whitehead, S.S. (2002). Genetic basis of attenuation of dengue virus type 4 small plaque mutants with restricted replication in suckling mice and in SCID mice transplanted with human liver cells. Virology *300*, 125–139.

Blome, S., Staubach, C., Henke, J., Carlson, J., and Beer, M. (2017). Classical swine fever—an updated review. Viruses *9*, 86.

Brecher, M., Li, Z., Liu, B., Zhang, J., Koetzner, C.A., Alifarag, A., Jones, S.A., Lin, Q., Kramer, L.D., and Li, H. (2017). A conformational switch high-throughput screening assay and allosteric inhibition of the flavivirus NS2B-NS3 protease. PLoS Pathog. *13*, e1006411.

Chambers, T.J., Droll, D.A., Tang, Y., Liang, Y., Ganesh, V.K., Murthy, K., and Nickells, M. (2005). Yellow fever virus NS2B-NS3 protease: characterization of charged-to-alanine mutant and revertant viruses and analysis of polyprotein-cleavage activities. J. Gen. Virol. *86*, 1403–1413.

Chung, J.Y., Lu, M., Yin, Q., Lin, S.-C., and Wu, H. (2007). Molecular basis for the unique specificity of TRAF6. Adv. Exp. Med. Biol. *597*, 122–130.

Dinkel, H., Van Roey, K., Michael, S., Davey, N.E., Weatheritt, R.J., Born, D., Speck, T., Kruger, D., Grebnev, G., Kuban, M., et al. (2013). The eukaryotic linear motif resource ELM: 10 years and counting. Nucleic Acids Res. *42*, D259–D266.

Eastman, P.S., and Blair, C.D. (1985). Temperature-sensitive mutants of Japanese encephalitis virus. J. Virol. *55*, 611–616.

Erbel, P., Schiering, N., D'Arcy, A., Renatus, M., Kroemer, M., Lim, S.P., Yin, Z., Keller, T.H., Vasudevan, S.G., and Hommel, U. (2006). Structural basis for the activation of flaviviral NS3 proteases from dengue and West Nile virus. Nat. Struct. Mol. Biol. *13*, 372–373.

Falgout, B., Pethel, M., Zhang, Y., and Lai, C.-J. (1991). Both nonstructural proteins NS2B and NS3 are required for the proteolytic processing of dengue virus nonstructural proteins. J. Virol. *65*, 2467–2475.

Frisch, M.J., Trucks, G., Schlegel, H., Scuseria, G.E., Robb, M.A., Cheeseman, J.R., Scalmani, G., Barone, G.A., Petersson, G.A., Nakatsuji, H., et al., Gaussian 09, Revision A.02, Gaussian Inc., 2009.

Geiss, B.J., Stahla, H., Hannah, A.M., Gari, H.H., and Keenan, S.M. (2009). Focus on flaviviruses: current and future drug targets. Future Med. Chem. *1*, 327–344.

Gentry, J.J., Rutkoski, N.J., Burke, T.L., and Carter, B.D. (2004). A functional interaction between the p75 neurotrophin receptor interacting factors, TRAF6 and NRIF. J. Biol. Chem. *279*, 16646–16656.

Hanley, K.A., Lee, J.J., Blaney, J.E., Murphy, B.R., and Whitehead, S.S. (2002). Paired charge-to-alanine mutagenesis of dengue virus type 4 NS5 generates mutants with temperature-sensitive, host range, and mouse attenuation phenotypes. J. Virol. *76*, 525–531.

Hermance, M.E., and Thangamani, S. (2017). Powassan virus: an emerging arbovirus of public health concern in North America. Vector-Borne Zoonotic Dis. *17*, 453–462.

Hou, W., Jin, Y.-H., Kang, H.S., and Kim, B.S. (2014). Interleukin-6 (IL-6) and IL-17 synergistically promote viral persistence by inhibiting cellular apoptosis and cytotoxic T cell function. J. Virol. *88*, 8479–8489.

Inoue, J.-I., Gohda, J., and Akiyama, T. (2007). Characteristics and biological functions of TRAF6. Adv. Exp. Med. Biol. *597*, 72–79.

Konno, H., Yamamoto, T., Yamazaki, K., Gohda, J., Akiyama, T., Semba, K., Goto, H., Kato, A., Yujiri, T., Imai, T., et al. (2009). TRAF6 establishes innate immune responses by activating NF-kappaB and IRF7 upon sensing cytosolic viral RNA and DNA. PLoS One *4*, e5674.

Leyssen, P., Clercq, E., and Neyts, J. (2000). Perspectives for the treatment of infections with *Flaviviridae*. Clin. Microbiol. Rev. *13*, 67–82.

Li, K., Phoo, W.W., and Luo, D. (2014). Functional interplay among the flavivirus NS3 protease, helicase, and cofactors. Virol. Sin. *29*, 74–85.

Liu, H., Zhang, L., Sun, J., Chen, W., Li, S., Wang, Q., Yu, H., Xia, Z., Jin, X., and Wang, C. (2017). Endoplasmic reticulum protein SCAP inhibits dengue virus NS2B3 protease by suppressing its K27-linked polyubiquitylation. J. Virol. *91*, 1–17.

Luo, D., Vasudevan, S., and Lescar, J. (2015). The flavivirus NS2B–NS3 protease–helicase as a target for antiviral drug development. Antiviral Res. *118*, 148–158.

Lv, H., Dong, W., Cao, Z., Li, X., Wang, J., Qian, G., Lv, Q., Wang, C., Guo, K., and Zhang, Y. (2017). TRAF6 is a novel NS3-interacting protein that inhibits classical swine fever virus replication. Sci. Rep. *7*, 6737.

Mao, L.S., Wang, Y.L., Liu, Y.M., and Hu, X.C. (2003). Multiple intermolecular interaction modes of positively charged residues with adenine in ATP-binding proteins. J. Am. Chem. Soc. *125*, 14216–14217.

Meads, M.B., Li, Z.W., and Dalton, W.S. (2010). A novel TNF receptor-associated factor 6 binding domain mediates NF- B signaling by the common cytokine receptor subunit. J. Immonol. *185*, 1606–1615.

Megas, C., Hatzivassiliou, E.G., Yin, Q., Marinopoulou, E., Hadweh, P., Vignali, D.A.A., and Mosialos, G. (2011). Mutational analysis of TRAF6 reveals a conserved functional role of the RING dimerization interface and a potentially necessary but insufficient role of RING-dependent TRAF6 polyubiquitination towards NF-κB activation. Cell Signal. *23*, 772–777.

Ning, S., Campos, A.D., Darnay, B.G., Bentz, G.L., and Pagano, J.S. (2008). TRAF6 and the three C-terminal lysine sites on IRF7 are required for its ubiquitination-mediated activation by the tumor necrosis factor receptor family member latent membrane protein 1. Mol. Cell. Biol. *28*, 6536–6546.

Noels, H., van Loo, G., Hagens, S., Broeckx, V., Beyaert, R., Marynen, P., and Baens, M. (2007). A Novel TRAF6 binding site in MALT1 defines distinct mechanisms of NF-κB activation by API2·MALT1 fusions. J. Biol. Chem. *282*, 10180–10189.

Palanisamy, N., Akaberi, D., and Lennerstrand, J. (2018). Protein backbone flexibility pattern is evolutionarily conserved in the Flaviviridae family: a case of NS3 protease in Flavivirus and Hepacivirus. Mol. Phylogenet. Evol. *118*, 58–63.

Pastorino, B.A.M., Peyrefitte, C.N., Grandadam, M., Thill, M.C.E., Tolou, H.J., and Bessaud, M. (2006). Mutagenesis analysis of the NS2B determinants of the Alkhurma virus NS2B-NS3 protease activation. J. Gen. Virol. *87*, 3279–3283.

Pu, J., Wu, S., Xie, H., Li, Y., Yang, Z., Wu, X., and Huang, X. (2017). miR-146a Inhibits dengue-virus-induced autophagy by targeting TRAF6. Arch. Virol. *162*, 3645–3659.

Rumyantsev, A.A., Murphy, B.R., and Pletnev, A.G. (2006). A tick-borne langat virus mutant that is temperature sensitive and host range restricted in neuroblastoma cells and lacks neuroinvasiveness for immunodeficient mice. J. Virol. *80*, 1427–1439.

Sharma, N., and Verma, R. (2015). miR-146a suppresses cellular immune response during Japanese encephalitis virus JaOArS982 strain infection in human microglial cells. J. Neuroinflammation *12*, 1–16.

Shi, Z., Zhang, Z., Zhang, Z., Wang, Y., Li, C., Wang, X., He, F., Sun, L., Jiao, S., Shi, W., and Zhou, Z. (2015). Structural Insights into mitochondrial antiviral signaling protein (MAVS)-tumor necrosis factor receptor-associated factor 6 (TRAF6) signaling. J. Biol. Chem. *290*, 26811–26820.

Stack, J., Hurst, T.P., Flannery, S.M., Brennan, K., Rupp, S., Oda, S., Khan, A.R., and Bowie, A.G. (2013). Poxviral protein A52 stimulates p38 mitogen-activated protein kinase (MAPK) activation by causing tumor necrosis factor receptor-associated factor 6 (TRAF6) self-association leading to transforming growth factor β-activated Kinase 1 (TAK1) Recruitment. J. Biol. Chem. *288*, 33642–33653.

Tautz, N., Kaiser, A., and Thiel, H.-J. (2000). NS3 serine protease of bovine viral diarrhea virus: characterization of active site residues, NS4A cofactor domain, and protease–cofactor interactions. Virology *273*, 351–363.

Tautz, N., Tews, B.A., and Meyers, G. (2015). The molecular biology of pestiviruses. Adv. Virus Res. *93*, 47–160.

Taylor, R.T., Lubick, K.J., Robertson, S.J., Broughton, J.P., Bloom, M.E., Bresnahan, W.A., and Best, S.M. (2011). TRIM79α, an interferon-stimulated gene product, restricts tick-borne encephalitis virus replication by degrading the viral RNA polymerase. Cell Host Microbe *10*, 185–196.

Verstak, B., Stack, J., Ve, T., Mangan, M., Hjerrild, K., Jeon, J., Stahl, R., Latz, E., Gay, N., Kobe, B., et al. (2014). The TLR signaling adaptor TRAM interacts with TRAF6 to mediate activation of the inflammatory response by TLR4. J. Leukoc. Biol. *96*, 427–436.

Walsh, M.C., Lee, J., and Choi, Y. (2015). Tumor necrosis factor receptor- associated factor 6 (TRAF6) regulation of development, function, and homeostasis of the immune system. Immunol. Rev. *266*, 72–92.

Wu, H., and Arron, J.R. (2003). TRAF6, a molecular bridge spanning adaptive immunity, innate immunity and osteoimmunology. BioEssays *25*, 1096–1105.

Wu, S., He, L., Li, Y., Wang, T., Feng, L., Jiang, L., Zhang, P., and Huang, X. (2013). miR-146a facilitates replication of dengue virus by dampening interferon induction by targeting TRAF6. J. Infect. *67*, 329–341.

Ye, H., Arron, J.R., Lamothe, B., Cirilli, M., Kobayashi, T., Shevde, N., Segal, D., Dzivenu, O., Vologodskaia, M., Yim, M., et al. (2002). Distinct molecular mechanism for initiating TRAF6 signalling. Nature *418*, 443–446.

Yoshida, R., Takaesu, G., Yoshida, H., Okamoto, F., Yoshioka, T., Choi, Y., Akira, S., Kawai, T., Yoshimura, A., and Kobayashi, T. (2008). TRAF6 and MEKK1 play a pivotal role in the RIG-I-like helicase antiviral pathway. J. Biol. Chem. *283*, 36211–36220.

Yu, J., Yun, H., Shin, B., Kim, Y., Park, E.-S., Choi, S., Yu, J., Amarasekara, D.S., Kim, S., Inoue, J.-I., et al. (2016). Interaction of tumor necrosis factor receptor-associated factor 6 (TRAF6) and Vav3 in the receptor activator of nuclear factor κB (RANK) Signaling complex enhances osteoclastogenesis. J. Biol. Chem. *291*, 20643–20660.

ISCI, Volume *15*

Supplemental Information

TRAF6 Plays a Proviral Role in Tick-Borne Flavivirus Infection through Interaction with the NS3 Protease

Brian H. Youseff, Thomas G. Brewer, Kristin L. McNally, Adaeze O. Izuogu, Kirk J. Lubick, John B. Presloid, Saad Alqahtani, Saurabh Chattopadhyay, Sonja M. Best, Xiche Hu, and R. Travis Taylor

SUPPLEMENTAL FIGURES

A

		NS3pro		TBM1		TBM2	
	Accession	% Identity	% Similarity	% Identity	% Similarity	% Identity	% Similarity
TBEV	AMP18887.1	100	100	100	100	100	100
LGTV	NP_620108.1	78	88	50	66	83	99
OHFV	NP_878909.1	90	95	83	96	83	99
LIV	NP_044677.1	92	96	100	100	83	99
ALKV	NC_004355.1	79	93	83	96	83	99
KFDV	AFF18436.1	79	92	83	96	83	99
POWV	AAL32169.1	73	86	66	99	16	32

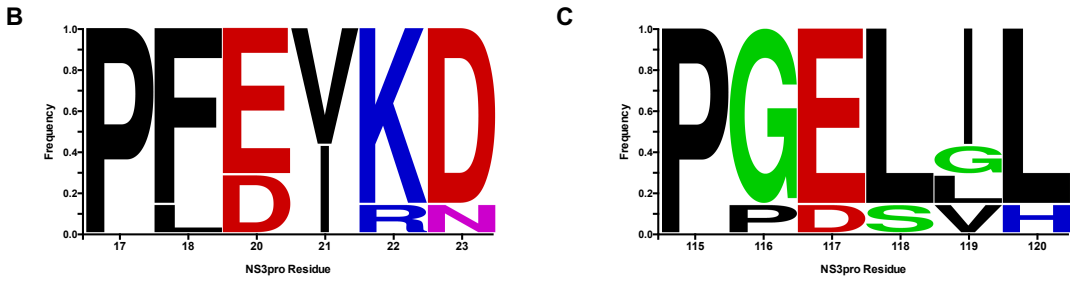

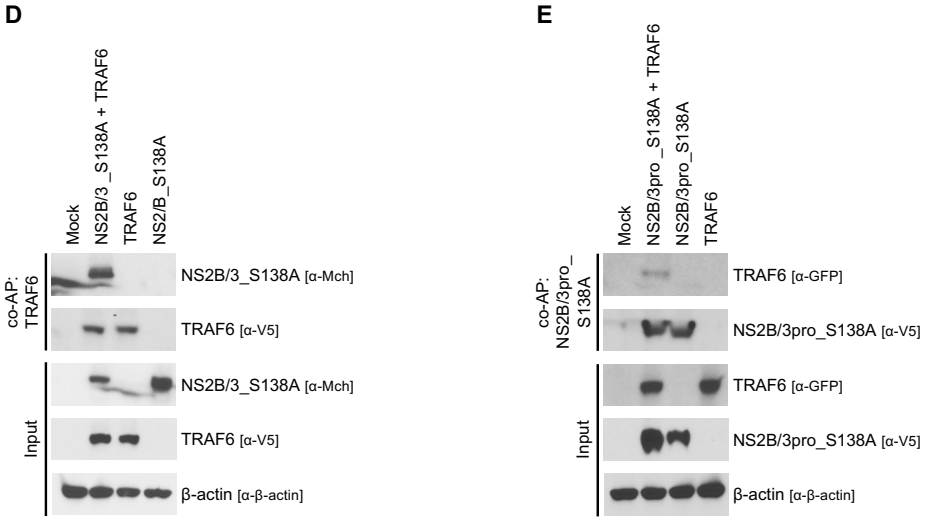

Figure S1. LGTV NS3pro interacts with TRAF6. Related to Figure 1.

(A) Sequence identity and similarity of NS3pro, TBM1, and TBM2 of TBFVs compared to TBEV.

(B) Sequence logo of TBM1.

(C) Sequence logo of TBM2.

(D-E) Co-AP of LGTV NS2B/3_S138A and LGTV NS2B/3pro_S138A constructs with TRAF6. HEK 293 cells were transfected with 2 µg of each indicated plasmid. Cell lysates were pulled down using streptavidin-conjugated beads at 24 hours post-transfection and eluted proteins were analyzed by immunoblot with indicated antibodies. Results representative of three independent experiments.

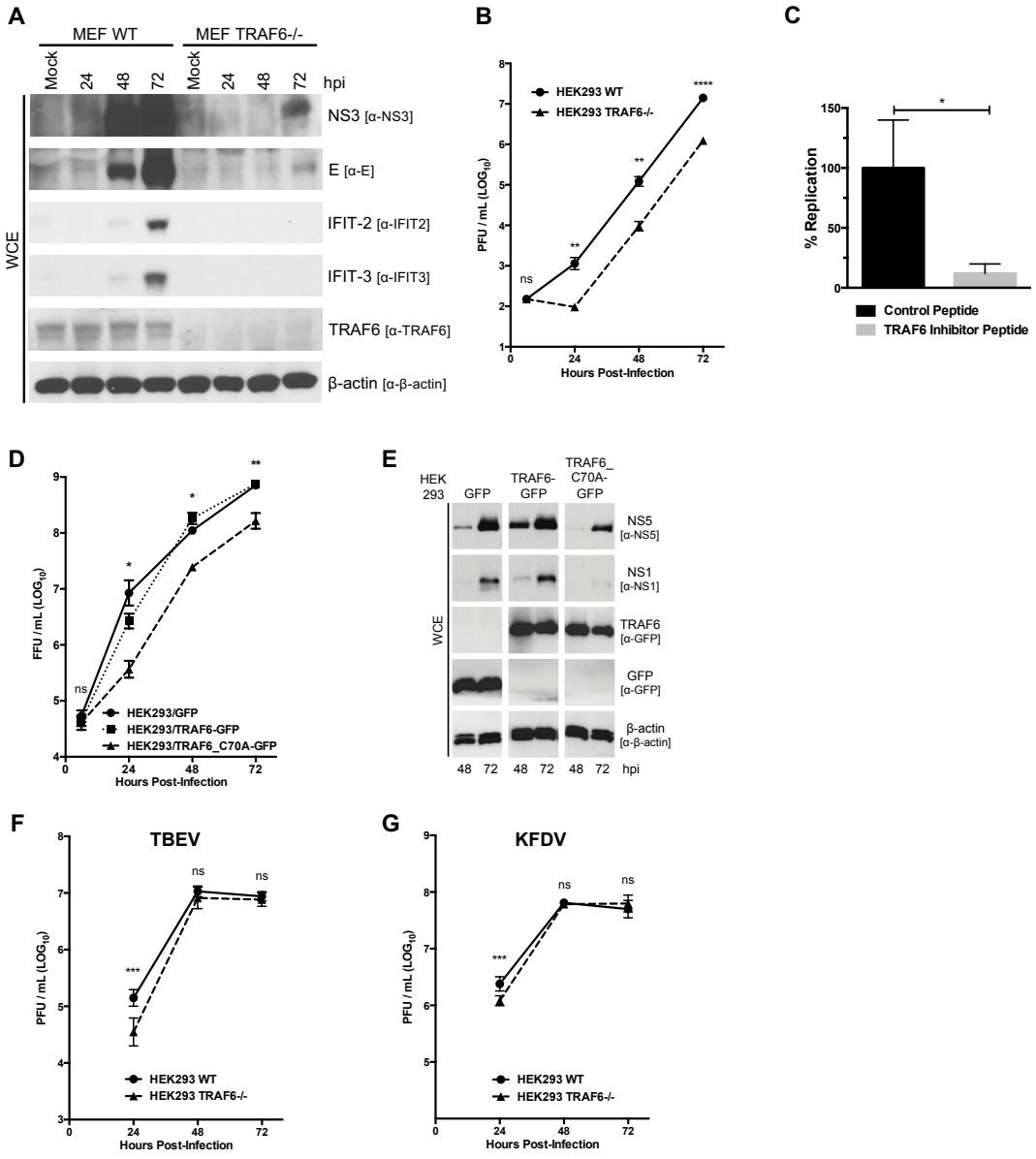

Figure S2. TRAF6 is a proviral factor for TBFVs. Related to Figure 2.

(A) Immunoblot analysis of whole cell extracts from WT or TRAF6$^{-/-}$ MEFs infected with LGTV (MOI 0.1) for indicated times (hr). Blots were probed with antibodies to LGTV NS3, LGTV E, IFIT2, IFIT3, TRAF6, and β-actin. Results representative of three or more independent experiments. Long exposures of LGTV NS3 and LGTV E are included in order to assess viral protein levels during infection of TRAF6$^{-/-}$ MEFs.

(B) Titration of infectious particles in the supernatant from WT or TRAF6$^{-/-}$ HEK 293 cells infected with LGTV (MOI of 0.1) for indicated times (hr). Virus titers were determined by plaque assay. Data are representative of three or more independent experiments performed in triplicate and plotted as mean +/- SEM. ns, not significant; **p<0.01; ****p<0.0001.

(C) Titration of infectious particles in the supernatant from HEK 293 cells pretreated with 150 μM TRAF6 inhibitor peptide or control peptide for 6 hr prior to infection with LGTV (MOI 1). Supernatants were collected at 48 hpi and titrated by immunofocus assay. Data are presented as percent replication relative to control peptide-treated cells. Data are representative of two independent experiments performed in triplicate and plotted as the mean +/- SEM. *p<0.05.

(D) Titration of infectious particles in the supernatant from HEK 293 cells stably expressing GFP, TRAF6-GFP, or TRAF6-C70A-GFP infected with LGTV (MOI of 10) for indicated times (hr). Virus titers were determined by immunofocus assay. Data are representative of three independent experiments performed in triplicate and plotted as mean +/- SEM. ns, not significant; *p<0.05; **p<0.01.

(E) Immunoblot analysis of whole cell extracts from the infected cells in (C) (48 and 72 hpi). Blots were probed with antibodies to LGTV NS5, LGTV NS1, GFP, and β-actin. Results representative of three independent experiments.

(F-G) Titration of infectious particles in the supernatant from WT or TRAF6$^{-/-}$ HEK 293 cells infected with TBEV (F) or KFDV (G) (MOI of 0.1) for indicated times (hr). Virus titers were determined by plaque assay. Data are average of three independent experiments performed in triplicate and plotted as mean +/- SEM. ns, not significant; ***p<0.001.

A

```
     Accession:
LGTV AAF75259  19 DVKNGVYRIYTPGLLWGQRQIGVGYGAKGVLHTMWHVTRGAALLVDGVAVGPYWADVREDVVCYGGAWSLESRWRG-ETVQVHAFPPGRA 107
MVEV CAA27184  71 DTTPGVYRIMARGILG-RYQAGVGVMHEGVFHTLWHTTRGAAIMSGEGRLTPYWGNVKEDRVTYGGPWKLDQKWNGVDDVQMIVVEPGKP 159
                  *   ***** . *.*  . * ***    ** **.** *****..      . ***  *.** *.*** * *. .* * . **.    **.

LGTV AAF75259 108 HETHQCQPGELILENGRKMGAIPIDLAKGTSGSPIMNSQGEVVGLYGNGLKT-NDTYVSSIAQG-EVEKSRPNLPQSVVGTGWTAKGQIT 195
MVEV CAA27184 160 AINVQTKPGIFKTAHG-EIGAVSLDYPIGTSGSPIVNSNGEIIGLYGNGVILGNGAYVSAIVQGERVEEPVP----EAYNPEMLKKRQLT 244
                    . *..**     .*  .**. .*   *******.**.**..******.   * .***.* **  **   *       .     * *.*

LGTV AAF75259 196 VLDMHPGSGKTHRVLPELIRQCVERRLRTLVLAPTRVVLREMERALSGKNVRFHSPAVTEQHANGAIVDVMCHATYVNRRLLPQGRQNWE 285
MVEV CAA27184 245 VLDLHPGAGKTRRILPQIIKDAIQKRLRTAVLAPTRVVAAEMAEALRGLPVRYLTPAVQREHSGNEIVDVMCHATLTHRLMSPLRVPNYN 334
                  ***.***.***.*.**..*. ....**** ********  **  ** *  **. .***  .*... *********  .* . *    *

LGTV AAF75259 286 VAIMDEAHWTDPHSIAARGHLYSLAKENRCAFVLMTATPPGKSEPFPESNGAIASEERQIPDGEWRDGFDWITEYEGRTAWFVPSIARGG 375
MVEV CAA27184 335 LFVMDEAHFTDPASIAARGYIATRVEAGEAAAIFMTATPPGTSDPFPDTNSPVHDVSSEIPDRAWSSGFEWITDYAGKTVWFVASVKMSN 424
                  . .***** *** ****** . .    . .* . ******* *.***..*  .     .***  *  **.***.* *.* *** *.   .

LGTV AAF75259 376 AIARALRQRGKSVICLNSKTFDKEYSRVKDEKPDFVVTTDISEMGANLDVTRVIDGRTNIKP---EEVDGRIELTGTRRVTTASAAQRRG 462
MVEV CAA27184 425 EIAQCLQRAGKRVIQLNRKSYDTEYPKCKNGDWDFVITTDISEMGANFGASRVIDCRKSVKPTILDEGEGRVILSVPSAITSASAAQRRG 514
                   **..*.. ** ** ** *..* ** . *    ***.**********   .**** *  .**   .* .**. *.    .*.********

LGTV AAF75259 463 RVGRQGGRT-DEYIYSGQCDDDDSGLVQWKEAQILLDNITTARGPVATFYGPEQERMTETAGHYRLPEEKRKHFRHLLAQCDFTPWLAWH 550
MVEV CAA27184 515 RVGRNPSQIGDEYHYGGGTSEDDTMLAHWTEAKILLDNIHLPNGLVAQLYGPERDKTYTMDGEYRLRGEERKTFLELIKTADLPVWLAYK 604
                  ****.  .  *** * * . .**. * .* **.******    * **  ****...     * ***  * ** *  *.  .*   *** .

LGTV AAF75259 551 VAANVASVTDRSWTWEGPEENAVDENNGELVTFRSPNGAERTLRPVWRDARMFREGRDIREFVSYASGRR 621
MVEV CAA27184 605 VASNGIQYNDRKWCFDGPRSNIILEDNNE-VEIITRIGERKVLKPRWLDARVYSDHQSLKWFKDFAAGKR 673
                  **.*    .** *. .**  * . * *.* *   .  *  . *.* * ***.. . . .. *  .*.*.*
```

B

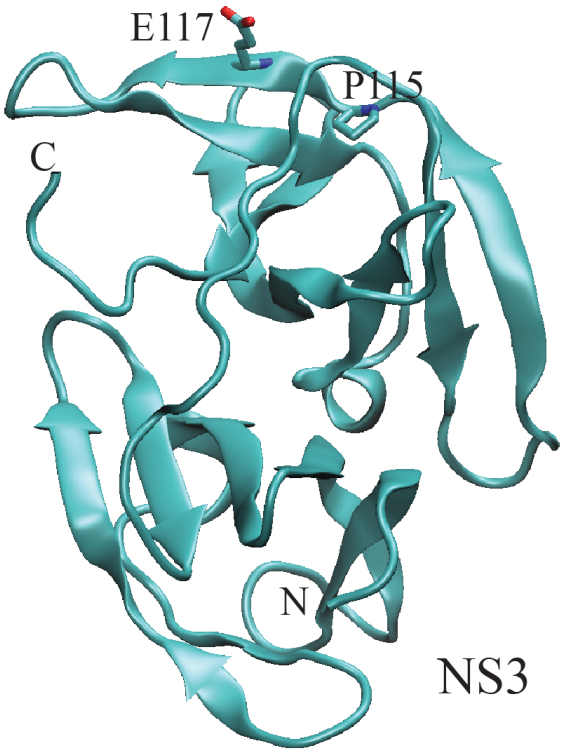

Figure S3. An E117A mutation in LGTV NS3pro disrupts TRAF6 binding and mature protease accumulation. Related to Figure 3.

(A) NS3pro sequence alignment between LGTV and MVEV. Terminal numbers of each sequence refer to residue position within NS3 protein. (*) indicates residues with the same identity; (.) indicates residues with similarity.

(B) The homology model of the LGTV NS3pro based on the 2.75 Å resolution x-ray crystal structure of NS3 from MVEV (PDB: 2WV9). TBM2 of LGTV NS3pro forms a beta strand that situates on the surface of the protein; two key residues P115 and E117 of TBM2 are shown.

TRANSPARENT METHODS

Cell culture and reagents. Human embryonic kidney (HEK) 293 cells, Vero cells, murine embryonic fibroblasts TRAF6$^{+/+}$ (WT MEF), murine embryonic fibroblasts TRAF6$^{-/-}$ (TRAF6$^{-/-}$ MEF) were grown in Dulbecco's modified enrichment medium (DMEM, Thermo Fisher Scientific) containing 10% (vol/vol) fetal bovine serum (FBS, Atlanta Biologicals), 100 units/ml penicillin, and 100 mg/ml streptomycin (Thermo Fisher Scientific) in an atmosphere of 5% CO_2 at 37°C. WT and TRAF6$^{-/-}$ MEFs were provided by Dr. S. Best (NIAID, NIH). All cells were counted on a Tali Image Cytometer (Invitrogen).

Isolation, culture, and immortalization of MEFs. Fifteen-day old C57BL/6 $^{+/-}$ mouse embryos were collected, washed with PBS, and torsos were removed. Torsos were washed with PBS, minced, placed in 0.05 % trypsin-EDTA (Invitrogen) containing 1 μg/ml DNase I (Ambion) and incubated at 37°C for 15 min. Cells were filtered using a 100 μM nylon strainer, centrifuged (500 x *g*, 5 min), resuspended in complete DMEM, and plated in tissue culture flasks (passage 1). Embryo genotypes were determined by TRAF6-specific PCR and only homozygote TRAF6$^{+/+}$ and TRAF6$^{-/-}$ cells were used in subsequent experiments. Cells were immortalized by knockdown of p53 using commercially-available lentivirus preparations (sc-29436-V, Santa Cruz Biotechnology). All animal experiments were done in compliance with the guidelines of the Animal Care and Use Committee of the NIH.

Generation of HEK 293 TRAF6 knock-out cells. WT HEK 293 cells (1 x 10^6 cells/well of a 6-well plate) were transfected with 2 μg of commercially available TRAF6 CRISPR/Cas9 knock-out plasmids (sc-400117, Santa Cruz Biotechnology) or Control CRISPR/Cas9 plasmid (sc-418922, Santa Cruz Biotechnology) using Lipofectamine 3000 Reagent (100022052, Invitrogen). The TRAF6 CRISPR/Cas9 knock-out plasmids consists of a pool of 3 plasmids, each encoding the Cas9 nuclease, a TRAF6-specific 20 nt guide RNA, and GFP marker. The Control CRISPR/Cas9 plasmid contains a non-targeting 20 nt scramble guide RNA and GFP marker. At 24 hours post-transfection (hpt) GFP was visualized to assess transfection efficiency, which was greater than 95%. Transfected cells were then isolated by serial dilution and plated in a 48-well plate. Individual wells were inspected by microscopy 4 days post-transfection to confirm the presence of a single clone and then allowed to continue to grow until reaching roughly 75% confluency. Cells were then trypsinized, equally divided, and plated in 2 wells of a 6-well plate. When cells reached 75% confluency, whole cell extract of each duplicate well was immunoblotted to confirm the absence of TRAF6 using α-TRAF6 (roughly 10% of clones did not express TRAF6). A single isolate was propagated and used for all subsequent studies. Furthermore, the

isolate was confirmed to have loss GFP expression (because lack of selection) by microscopy and immunoblot.

Antibodies. The following antibodies were used: α-β-actin (AM4302, Ambion); α-GFP (632381, Clontech and ab32146, Abcam); α-DsRed (632496, Clontech); α-V5 (46-0705, Invitrogen); α-HA (16B12, Covance); α-TRAF6 (ab33915, Abcam); α-TBEV (VR79; ATCC); affinity purified chicken α-LGTV NS3 and control IgY antisera (custom prepared by Aves Labs and α-LGTV NS3 (provided by Dr. S. Best, NIAID, NIH, (Taylor et al., 2011)); α-LGTV E and α-LGTV NS1 (provided by Dr. C. Schmaljohn, USAMRIID); α-WNV NS3 (R&D Systems, MAB2907); α-IFIT2 and α-IFIT3 (provided by Dr. S. Chattopadhyay, University of Toledo (Chattopadhyay et al., 2016)).

Virus infections. The following viruses were used in this study: Langat virus (LGTV, strain TP21, provided by Dr. A. Pletnev, NIAID, NIH), tick-borne encephalitis virus (TBEV, strain Sofjin, provided by Dr. M. Holbrook, NIAID, NIH), Kyasanur Forest disease virus (KFDV, provided by Dr. S. M. Best, NIAID, NIH), West Nile virus (WNV, strain NY99, provided by Dr. S. M. Best, NIAID, NIH), Kunjin virus (KUNV, provided by Dr. S. M. Best, NIAID, NIH). All virus stocks were propagated on Vero cells. LGTV was titrated by immunofocus assay or plaque assay as indicated and TBEV, KFDV, KUNV, and WNV were titrated by plaque assay. All procedures with WNV were performed under biosafety level-3 (BSL-3) conditions at the Rocky Mountain Laboratories Integrated Research Facility (RML, Hamilton, MT). All procedures with TBEV and KFVD were performed under BSL-4 conditions at RML. Multiplicity of infection (MOI) is represented as focus forming units (FFU) or plaque forming units (PFU) per cell.

Immunofocus assay. Cells were infected with LGTV at indicated MOI and viral supernatants collected at various time points post-infection. All samples were stored at -80°C until time of titration. 24 hr prior to set up, 24-well plates were seeded with 2×10^5 Vero cells per well. 250 µL of 10-fold dilutions of viral supernatants (ranging from 10^0 to 10^{-8}, depending on MOI) were added to individual wells. After a 1 hr adsorption period, the inoculum was removed, and the cells were overlaid with DMEM containing 0.8% methylcellulose (w/v) and 2% (vol/vol) FBS. At 5 days post-adsorption, wells were washed twice with DPBS and fixed with 100% methanol for 20 min at room temperature (RT). Plates were washed twice with DPBS and blocked with Opti-MEM (31985-070, Thermo Fisher Scientific) for 30 min at RT. Blocking Opti-MEM was removed and α-LGTV E (1:1000) and α-LGTV NS1 (1:1000) in Opti-MEM added to each well. Plates were incubated for 1 hr at 37°C, washed twice with DPBS, and then incubated with horseradish peroxidase (HRP)-conjugated goat anti-mouse antibody (1:1000, A28177, Thermo Fisher Scientific) in Opti-MEM for 1 hr at 37˚C. Plates were washed twice with PBS and FFUs

were visualized by adding freshly prepared peroxidase solution containing 0.4 mg/ml 3,3′-diaminobenzidine (D5637, Sigma) and 0.0135% hydrogen peroxide in DPBS.

Plaque assay. Cells were infected with KUNV, WNV, KFDV, or TBEV at indicated MOI and viral supernatants collected a various time points post-infection. All samples were stored at -80°C until time of titration. 24 hr prior to set-up, 24-well plates were seeded with 2 x 10^5 Vero cells per well. 250 µL of 10-fold dilutions of viral supernatants (ranging from 10^0 to 10^{-10}, depending on MOI) were added to individual wells. After a 1 hr adsorption period, the inoculum was removed, and the cells were overlaid with Minimum Essential Medium (MEM, 10370-021, Thermo Fisher Scientific) containing 1.5% carboxymethylcellulose (w/v, C4888, Sigma). At 4 days post-adsorption, cells were fixed with 10% formaldehyde for 1 hr at RT and then washed with water to remove all residual overlay media. To visualize plaques, crystal violet solution (1% crystal violet in 25% ethanol) was added to each well and incubated for 15 min at RT and then washed extensively to remove residual crystal violet.

Immunofluorescence confocal microscopy. Cells were plated in 8-well Lab-Tek II chamber slides (154534, Thermo Fisher Scientific) and prepared by washing twice with DPBS before fixing with fresh 4% paraformaldehyde (43368, Alfa Aesar) for 20 min at RT. Cells were washed 3 times with DPBS-T (PBS, 0.5% Tween-20) and then incubated with permeabilization buffer (0.1% Triton X-100, 0.1% sodium citrate) for 5 min at RT. Slides were blocked in DPBS, 0.5% BSA, 1% goat serum for 1 hr at RT. Cells were then incubated with primary antibody for 1 hr at RT, washed 3 times with DPBS-T and incubated with appropriate secondary antibodies conjugated to Alexa Fluor 488 or Alexa Fluor 594 (A11029, A11042, Thermo Fisher Scientific) for 1 hr at RT. Slides with GFP were stained with anti-GFP conjugated to Alexa Fluor 488 (A21311, Thermo Fisher Scientific). Slides were washed 3 times with DPBS-T in the dark and overlaid with glass coverslips using Prolong Gold Antifade Reagent with DAPI (P36931, Thermo Fisher Scientific). Stained cells were visualized using an Olympus confocal microscope (Olympus Fluoview FV1000).

Immunoblotting. Cells were washed twice in DPBS and harvested in 1 mL radioimmunoprecipitation assay (RIPA) buffer (50 mM Tris-HCl, 150 mM NaCl, 0.1 % SDS, 1% NP-40, 0.5% Na-deoxycholate) with Pierce Protease Inhibitor Tablets, EDTA Free (PI, 88266, Thermo Fisher Scientific). To ensure complete lysis, samples were subjected to three snap freeze/thaw cycles in liquid nitrogen. Samples were treated with 10 units of Turbo DNAse (AM2238, Thermo Fisher Scientific) and insoluble cellular debris was removed by centrifugation (10000 x *g* for 10 min at 4°C). Protein concentration of samples was determined by DC Protein Assay (5000111, Bio-Rad). Equal amounts (10-

30 µg) of protein in sample buffer (2X SB, 62.5 mM TRIS pH 6.8, 10% glycerol, 15 mM EDTA, 4% 2-ME, 2% SDS, and bromophenol blue) were incubated for 10 min at 95°C and loaded on a 10% polyacrylamide gel and resolved by electrophoresis. Protein was transferred onto a nitrocellulose membrane using the iBlot Gel Transfer Device (Thermo Fisher Scientific) and blocked in 5% milk in PBS-T. Membranes were probed with specific primary antibodies overnight at 4˚C followed by a secondary incubation with HRP-conjugated goat anti-mouse antibody (1:3,000, A28177, Thermo Fisher Scientific), anti-rabbit IgG (1:3,000, A27086, Thermo Fisher Scientific), or anti-chicken antibodies (1:3,000, H-1004, Aves Laboratory) for 1 hr at RT. Immunoreactive proteins were detected using Pierce ECL Plus Western Blotting Substrate (32132, Thermo Fisher Scientific) and exposed to film. Quantification of immunoblot bands was performed using ImageJ software (version 1.50i, (Campbell and Pletnev, 2000)).

Co-immunoprecipitation assay (co-IP). HEK 293 cells (1 x1 0^6 cells/well of a 6-well plate) were transfected with 2 µg of indicated plasmid with Lipofectamine 3000 reagent (100022052, Invitrogen). At 24 hpt, cells were infected with LGTV or KUNV at a MOI of 10. At 24 hours post-infection (hpi), cells were washed twice with DPBS and harvested in 1 mL immunoprecipitation wash buffer (WB1, 50 mM Tris-HCl pH 7.5, 150mM NaCl, 1% NP-40, and 0.5% Na-deoxycholate, and PI). To ensure complete lysis, samples were subjected to three snap freeze/thaw cycles in liquid nitrogen. Samples were treated with 10 units of Turbo DNAse and insoluble cellular debris was removed by centrifugation (10000 x *g* for 10 min at 4°C). 100 µL of sample was reserved for input analysis. Samples were incubated with Pierce Control Agarose Resin (26150, Thermo Fisher Scientific) for 3 hr at 4°C with rotation as a pre-clear step. After pre-clearing, the samples were incubated with indicated 2 µg of primary antibody for 1 hr at 4°C with rotation then incubated with 50 µL of Protein A-conjugated Agarose Beads (15918-014, Invitrogen) overnight at 4°C with rotation. For co-IP using chicken antibodies, PrecipHen beads (Aves Labs) were used for both pre-clear and precipitation steps. The beads were washed 3 times in RIPA buffer for 15 min at 4°C with rotation followed by elution in 50 µL 2X SB and incubated for 15 min at 95°C. The eluted samples were assayed by immunoblotting as described above.

Co-affinity purification assay (co-AP). As described previously (Taylor et al., 2011), HEK 293 cells (1 x 10^6 cells/well of a 6-well plate) were transfected with 2 µg of indicated plasmids with Lipofectamine 3000 Reagent (100022052, Invitrogen). Vector DNA was used as a transfection filler where appropriate. At 24 hpt, cells were then washed twice with DPBS and harvested in 1 mL WB1 with PI. To ensure complete lysis, samples were subject to three snap freeze/thaw cycles in liquid nitrogen. Samples were treated with 10 units of Turbo DNAse and insoluble cellular debris was removed by centrifugation

(10000 x *g* for 10 min at 4°C). 100 µL of sample was reserved for input analysis. Samples were incubated with Pierce Control Agarose Resin for 3 hr at 4°C with rotation as a pre-clear step. After pre-clearing, the samples were incubated with streptavidin-conjugated agarose beads (S951, Thermo Fisher Scientific) overnight at 4°C with rotation. The beads were washed 3 times in RIPA buffer for 15 min at 4°C with rotation followed by elution in 50µL 2X SB incubated for 15 min at 95°C. The eluted samples were assayed by immunoblotting as described above.

Enzyme linked immunosorbant assay (ELISA). Interferon-β (IFN-β) in culture supernatants of LGTV-infected cells was quantified by VeriKine Mouse IFN-β ELISA Kit (42400-1, PBL Assay Science) according to manufacturer's protocol. ELISA plates were read on a CLARIOstar plate reader (BMG Labtech).

Infectious clone technology. A sub-cloning vector was constructed by PCR amplification of the region between the endogenous restriction sites, NsiI and SpeI found in the full-length plasmid DNA p61-E5 corresponding to LGTV strain E5 (provided by Dr. A. Pletnev, NIAID, NIH, (Campbell and Pletnev, 2000; Pletnev, 2001; Rumyantsev et al., 2006)) followed by ligation into the Gateway entry vector, pENTR-SD-D-TOPO (46-0823,Thermo Fisher Scientific) according to manufacturer's protocol. Site-directed mutagenesis of sub-cloning vector was performed with QuikChange II Site-Directed Mutagenesis Kit (200523-5, Agilent Technologies). Desired mutations were confirmed by sequencing followed by cloning of mutation into the LGTV infectious clone. Mutated full-length infectious clone was linearized by EcoRV digestion for 4 hr at 37 ˚C and cleaned up by ethanol precipitation to remove contaminants. Linearized DNA was used as a template for *in vitro* transcription using the MEGAscript SP6 polymerase kit (AM1330, Ambion) with 15 mM m^7G cap analog (AM8048, Ambion) according to the manufacturer's protocol. The resultant RNA was treated with DNAse to remove DNA contamination. HEK 293 cells were transfected with viral RNA using Lipofectamine 3000. At 6 days post-transfection cell culture supernatant was collected, filtered, and concentrated by ultracentrifugation to produce mutant virus stocks. Each mutant viral stock was titrated by immunfocus assay on Vero cells. Additionally, viral RNA was isolated from each stock using QIAamp Viral RNA Mini Kit (52906, Qiagen), reverse transcribed using Superscript Reverse Transcriptase, and sequenced to confirm presence of mutation.

Bioinformatics. Viral sequences were obtained from the National Center for Biotechnology Information databases (https://www.ncbi.nlm.nih.gov). Accession numbers for each sequence are provided in corresponding figure or table. Eukaryotic Linear Motif (ELM) analysis of the TBEV polyprotein was performed with the ELM

Resource for Functional Sites in Proteins (http://elm.eu.org, (Dinkel et al., 2013)). Sequence alignments and calculations of sequence percent identity/similarity were made using MacVector version 12.7.0. Sequence logos of TBMs were generated with WebLogo version 2.8.2 (http://weblogo.berkeley.edu/logo.cgi, (Crooks et al., 2004)).

Molecular modeling of the TRAF6-NS3pro binding. A 3D structural model for the TRAF6-NS3pro complex was generated using a two-stage protocol. For the first stage, the three-dimensional structure for NS3pro from LGTV was predicted by means of homology modeling using the SWISS-MODEL Workplace (Arnold et al., 2006) because no crystal structure exists for any TBFV NS3pro. Murray Valley encephalitis virus (MVEV) NS3pro was used as a template for modeling because it was found to have the highest sequence identity (46%) among solved MBFV NS3pro crystal structures (Figure S3A). This high sequence homology lays the foundation for the generation of a reliable homology model for LGTV NS3pro based on the 2.75 Å resolution x-ray crystal structure of NS3pro from MVEV (PDB: 2WV9, (Assenberg et al., 2009)). Figure S3B displays the modeled structure of the LGTV NS3pro.

During the second stage, TBM2 of the model LGTV NS3pro structure was docked with the C-terminal MATH domain of TRAF6 from *Homo sapiens* by means of quantum mechanics/molecular mechanics (QM/MM) optimization to form the TRAF6-LGTV NS3pro complex. Initially, TBM2 of the model LGTV NS3pro structure was placed into the binding site of TRAF6 utilizing the crystal structure of a previously reported TRAF6-MAVS complex (PDB: 4Z8M, (Shi et al., 2015)) as a template. The QM layer contained TBM2 and its directly interacting protein residues of TRAF6 and was treated at the PM3 level. The MM layer included the rest of the TRAF6 protein and was described by the AMBER force field. The QM/MM optimization was performed using the Gaussian 09 package (Frisch et al., 2009). The QM/MM two-layer partitioning was carried out as previously described (Liu and Hu, 2006). The modeled structure of the complex of the TBM2 motif of LGTV NS3pro with the C-terminal MATH domain of TRAF6 is shown in Figure 3E.

The intermolecular interaction energies between E117 of LGTV NS3pro and its interacting protein partners in TRAF6 were calculated at the MP2/6-311++G** level using the supermolecular approach as previously described (Mao et al., 2003). In the supermolecular approach, the intermolecular interaction energy between the two monomeric molecules (e.g. A and B) is computed as the difference between the energy of the interacting dimer E_{AB} and the energies of the monomers E_A and E_B: $\Delta E_{int} = E_{AB} - E_A - E_B$. The basis set superposition error (BSSE) was corrected by the Boys and Bernardi Counter Poise Method (Boys and Bernardi, 1970). All calculations were carried out using the Gaussian09 software (Frisch et al., 2009). For the gas phase interaction energy ΔE^{gas}, the electronic energies for all molecular species (E_i, i=AB, A, B) are calculated directly. For

the aqueous phase interaction energy $\Delta E^{solution}$, the Polarizable Continuum (PCM) model was adopted. In a similar manner, the intermolecular interaction energies between the mutated A117 of NS3 and its interacting protein partners were calculated.

Statistical analysis. Data were analyzed by unpaired *t* tests using GraphPad Prism 6 software.

SUPPLEMENTAL REFERENCES

Arnold, K., Bordoli, L., Kopp, J., Schwede, T., 2006. The SWISS-MODEL workspace: a web-based environment for protein structure homology modelling. Bioinformatics 22, 195–201. doi:10.1093/bioinformatics/bti770

Assenberg, R., Mastrangelo, E., Walter, T.S., Verma, A., Milani, M., Owens, R.J., Stuart, D.I., Grimes, J.M., Mancini, E.J., 2009. Crystal Structure of a Novel Conformational State of the Flavivirus NS3 Protein: Implications for Polyprotein Processing and Viral Replication. Journal of Virology 83, 12895–12906. doi:10.1128/jvi.00942-09

Boys, S.F., Bernardi, F., 1970. The calculation of small molecular interactions by the differences of separate total energies. Some procedures with reduced errors. Molecular Physics 19, 553–566. doi:10.1080/00268977000101561

Campbell, M.S., Pletnev, A.G., 2000. Infectious cDNA Clones of Langat Tick-Borne Flavivirus That Differ from Their Parent in Peripheral Neurovirulence. Virology 269, 225–237. doi:10.1006/viro.2000.0220

Chattopadhyay, S., Kuzmanovic, T., Zhang, Y., Wetzel, J.L., Sen, G.C., 2016. Ubiquitination of the Transcription Factor IRF-3 Activates RIPA, the Apoptotic Pathway that Protects Mice from Viral Pathogenesis. Immunity 1–12. doi:10.1016/j.immuni.2016.04.009

Crooks, G.E., Hon, G., Chandonia, J.-M., Brenner, S.E., 2004. WebLogo: a sequence logo generator. Genome Research 14, 1188–1190. doi:10.1101/gr.849004

Dinkel, H., Van Roey, K., Michael, S., Davey, N.E., Weatheritt, R.J., Born, D., Speck, T., Kruger, D., Grebnev, G., Kuban, M., Strumillo, M., Uyar, B., Budd, A., Altenberg, B., Seiler, M., Chemes, L.B., Glavina, J., Sanchez, I.E., Diella, F., Gibson, T.J., 2013. The eukaryotic linear motif resource ELM: 10 years and counting. Nucleic Acids Research 42, D259–D266. doi:10.1093/nar/gkt1047

Frisch, M.J., Trucks, G., Schlegel, H., Scuseria, G.E., Robb, M.A., Cheeseman, J.R., Scalmani, G., Barone, G.A., Petersson, G.A., Nakatsuji, H., Caricato, M., Li, M., 2009. Gaussian 09.

Liu, Y.M., Hu, X.H., 2006. Molecular determinants for binding of ammonium ion in the ammonia transporter AmtB - A quantum chemical analysis 110, 1375–1381. doi:10.1021/jp054261c

Mao, L.S., Wang, Y.L., Liu, Y.M., Hu, X.C., 2003. Multiple intermolecular interaction modes of positively charged residues with adenine in ATP-binding proteins. J. Am. Chem. Soc. 125, 14216–14217. doi:10.1021/ja036096p

Pletnev, A.G., 2001. Infectious cDNA Clone of Attenuated Langat Tick-Borne Flavivirus (Strain E5) and a 3′ Deletion Mutant Constructed from It Exhibit Decreased Neuroinvasiveness in Immunodeficient Mice. Virology 282, 288–300. doi:10.1006/viro.2001.0846

Rumyantsev, A.A., Murphy, B.R., Pletnev, A.G., 2006. A Tick-Borne Langat Virus Mutant That Is Temperature Sensitive and Host Range Restricted in Neuroblastoma Cells and Lacks Neuroinvasiveness for Immunodeficient Mice. Journal of Virology 80, 1427–1439. doi:10.1128/JVI.80.3.1427-1439.2006

Shi, Z., Zhang, Z., Zhang, Z., Wang, Y., Li, C., Wang, X., He, F., Sun, L., Jiao, S., Shi, W., Zhou, Z., 2015. Structural Insights into mitochondrial antiviral signaling protein (MAVS)-tumor necrosis factor receptor-associated factor 6 (TRAF6) signaling. Journal of Biological Chemistry 290, 26811–26820. doi:10.1074/jbc.M115.666578

Taylor, R.T., Lubick, K.J., Robertson, S.J., Broughton, J.P., Bloom, M.E., Bresnahan, W.A., Best, S.M., 2011. TRIM79**a**, an Interferon-Stimulated Gene Product, Restricts Tick-Borne Encephalitis Virus Replication by Degrading the Viral RNA Polymerase. Cell Host Microbe 10, 185–196. doi:10.1016/j.chom.2011.08.004